ERDC/CHL TR-07-10

US Army Corps
of Engineers®
Engineer Research and
Development Center

Urban Flood Damage Reduction and Channel Restoration Demonstration Program for Arid and Semi-Arid Regions

Lateral Inflow in Supercritical Flow

Richard L. Stockstill

September 2007

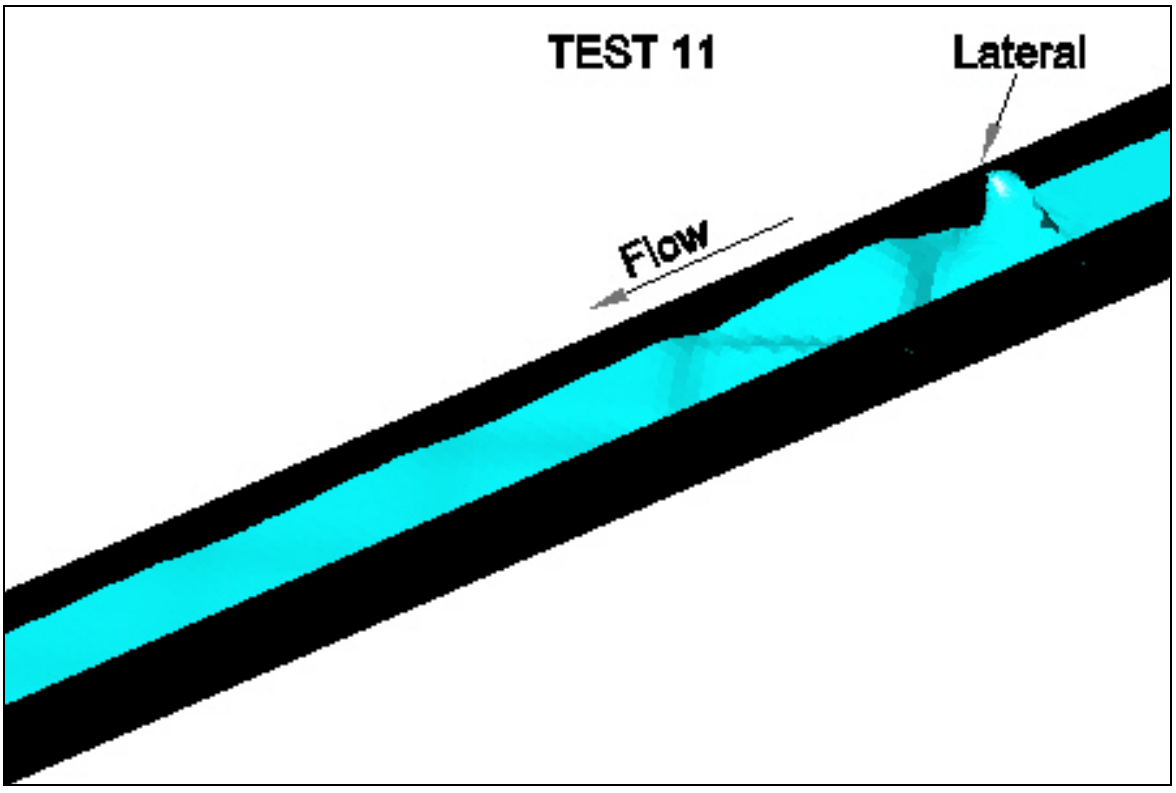

Coastal and Hydraulics Laboratory

Urban Flood Damage Reduction and
Channel Restoration Demonstration
Program for Arid and Semi-Arid Regions

ERDC/CHL TR-07-10
September 2007

Lateral Inflow in Supercritical Flow

Richard L. Stockstill

Coastal and Hydraulics Laboratory
U.S. Army Engineer Research and Development Center
3909 Halls Ferry Road
Vicksburg, MS 39180-6199

Final report

Prepared for U.S. Army Corps of Engineers
Washington, DC 20314-1000

Abstract: Lateral culverts are used to introduce storm drain flow into urban channels if the culvert flow is less than 10 percent of the main channel flow. Confluences of supercritical flow are complicated by standing waves that are generated at boundary alignment changes. The confluence addressed in this report is the case where culvert flow is introduced into a rectangular-shaped channel via a lateral. Even when the culvert discharge is less than 10 percent of the main channel flow, the momentum effects can produce significant bulking of the main channel flow. An understanding of the flow conditions in the vicinity of laterals is essential in an economical design of these structures. The current research evaluated a modeling method to determine if it is appropriate for simulating the flow depth increases attributed to lateral inflows in high-velocity channels. This report describes a series of laboratory experiments followed by numerical simulations. Following model validation, various geometric and hydraulic conditions were studied to evaluate hydraulic conditions such as location and magnitude of peak depths. Knowledge of these flow conditions is necessary for hydraulic design of channel walls (height and length) required to contain flows in the vicinity of laterals.

Contents

Figures and Tables

Figures

Tables

Preface

The research presented in this report was sponsored as part of the Urban Flood and Channel Restoration Demonstration Program for Arid and Semi-Arid Regions (UFDP). This work was conducted in the Coastal and Hydraulics Laboratory (CHL) of the U.S. Army Engineer Research and Development Center (ERDC) during the period of April 2004 to September 2006 under the direction of Thomas W. Richardson, Director, CHL; Dr. Rose Kress, Chief of the Navigation Division, CHL; and Dennis W. Webb, Chief of the Navigation Branch, CHL.

This investigation of lateral inflow in high-velocity channels was conducted by Dr. Richard L. Stockstill of the Navigation Branch, CHL. Acknowledgments are made to Meg Jonas, River Engineering Branch, CHL; Dr. Jennifer G. Duan, Desert Research Institute; Gale W. Fraser, General Manager/Chief Engineer, Clark County (Nevada) Regional Flood Control District (CCRFCD); and Stephen C. Roberts, Engineering Manager, CCRFCD, for their guidance in this study. Dr. R. C. (Charlie) Berger, CHL; Rene Vermeeren, Los Angeles District; and Scott Stonestreet, Sacramento District, provided peer review of the report.

COL Richard B. Jenkins was Commander and Executive Director of ERDC. Dr. James R. Houston was Director.

Unit Conversion Factors

Multiply	By	To Obtain
cubic feet	0.02831685	cubic meters
degrees (angle)	0.01745329	radians
feet	0.3048	meters
inches	0.0254	meters

1 Introduction

The main concern in evaluating high-velocity channels is the depth of flow in the channel for the design discharge. The depth must be known to determine sidewall heights and minimum bridge soffit elevations. Determining the depth of flow is complicated by side inflows and boundary features such as contractions, expansions, curves, and obstructions to the flow such as bridge piers and vehicle access ramps. These boundary features in a supercritical channel cause flow disturbances, which can result in a significant increase in the local flow depth. An accurate prediction of the water surface shape (i.e., variations in local depth) is essential for successfully evaluating a high-velocity channel.

The storm drain flow is typically introduced as a circular pipe having a flap gate (to prevent backflow) as shown Figure 1. The layout of a storm drain is complicated by the fact that generally these confluences occur near road crossings, where utilities and right-of-way constraints limit geometric flexibility in design. Lateral culverts are allowed if the culvert flow is less than 10 percent of the main channel flow. If the tributary flow is larger than 10 percent of the main channel flow rate, then a confluence is constructed according to EM 1110-2-1601 (U.S. Army 1991). The U.S. Army Engineer District, Los Angeles, requires 4 ft (1.2 m) of main channel flow submergence over lateral culverts. The Los Angeles District's geometric layout for laterals is shown in Figures 2 and 3. In many situations the culvert diameter is too large relative to the channel depth, so the 4-ft submergence can only be obtained by construction of a manifold system. These manifolds have multiple yet smaller ports and therefore meet the submergence requirements. However, these multiported manifolds are subject to collecting debris during flow events (Figure 4). Removal of this debris can be a labor-intensive maintenance effort.

Figure 1. Lateral inflow pipe with flap gate.

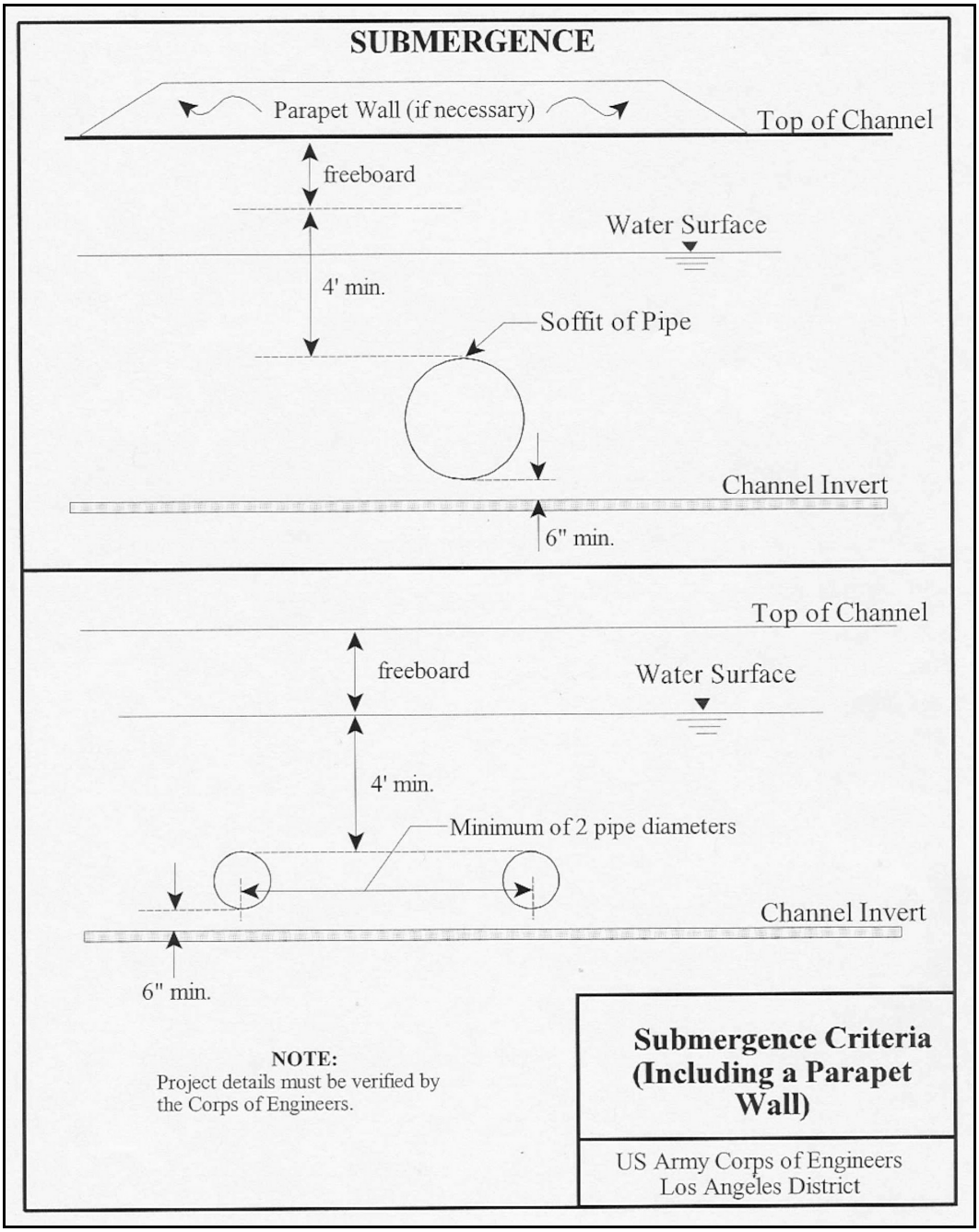

Figure 2. Attachment 1 from Los Angeles District's H & H Memorandum Number 1.

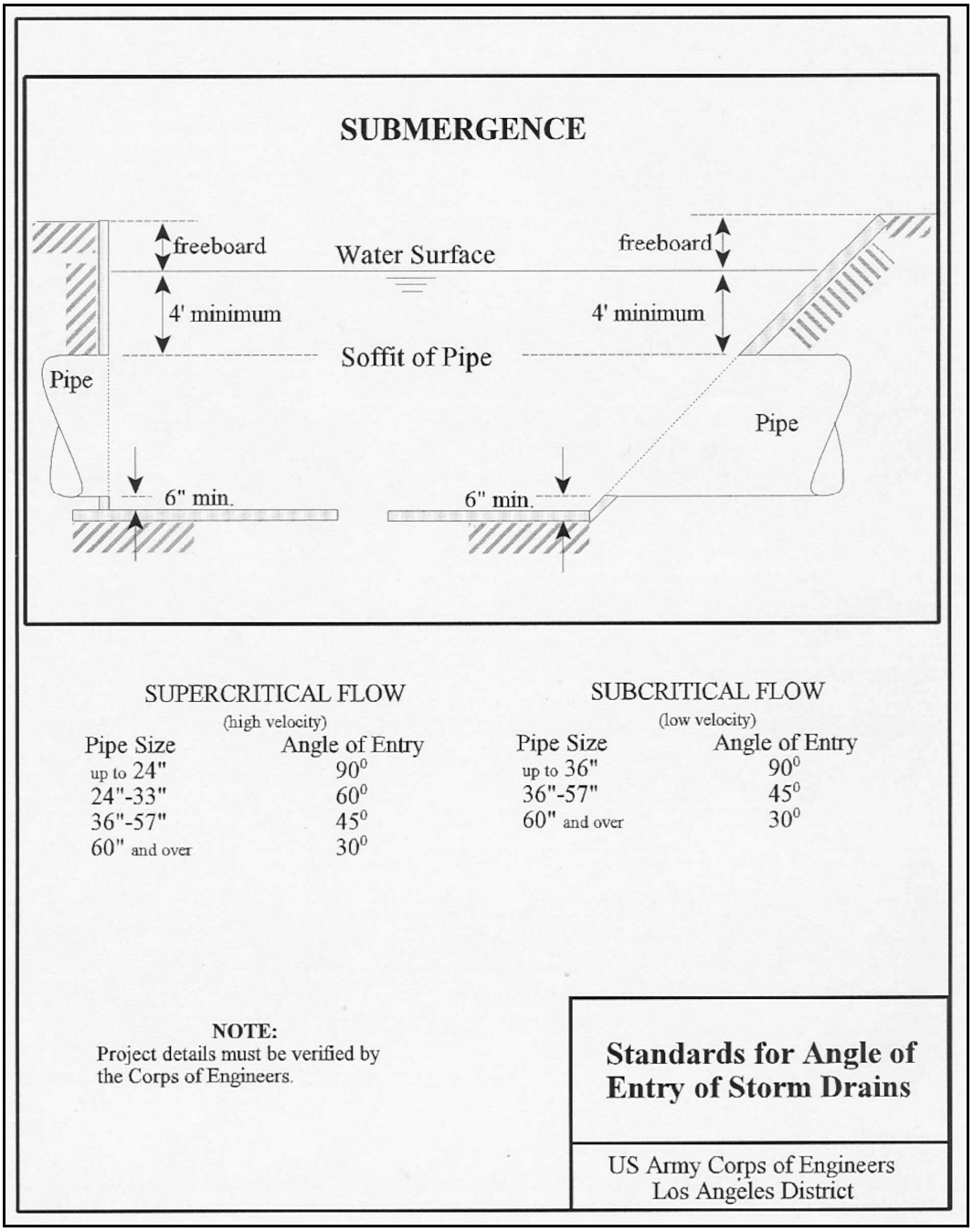

Figure 3. Attachment 2 from Los Angeles District's H & H Memorandum Number 1.

Figure 4. Lateral face on channel wall, with debris caught in the lateral outlet ports.

Confluences of supercritical flow are complicated by the fact that standing waves are generated at boundary alignment changes. The confluence addressed in this paper is the case where culvert flow is introduced into the main channel in a lateral.

The primary geometric and flow variables found at a lateral junction in an urban channel are shown in Figure 5. Dr. Jennifer Duan, Desert Research Institute, worked with Gale Fraser and Stephen Roberts, Clark County (Nevada) Regional Flood Control District (CCRFCD), to establish reasonable values of these parameters that are applicable to the CCRFCD's projects. The 100-year design flow discharge in the main channel (Q_1) varies from 2,300 to 11,500 cfs (65.1 to 325 cms). Rectangular channels generally have widths ranging from 13 to 80 ft (4 to 24 m). The bottom widths of trapezoidal channels vary from 10 to 60 ft (3 to 18 m), and they have side slopes of 2H:1V. The lateral inflow rate (Q_2) must be less than 10 percent of the main channel discharge (i.e., $0 \le Q_2 \le 0.1\ Q_1$). The invert of the lateral is set about 6 in. (0.15 m) above the invert of the main channel (i.e., P = 0.5 ft).

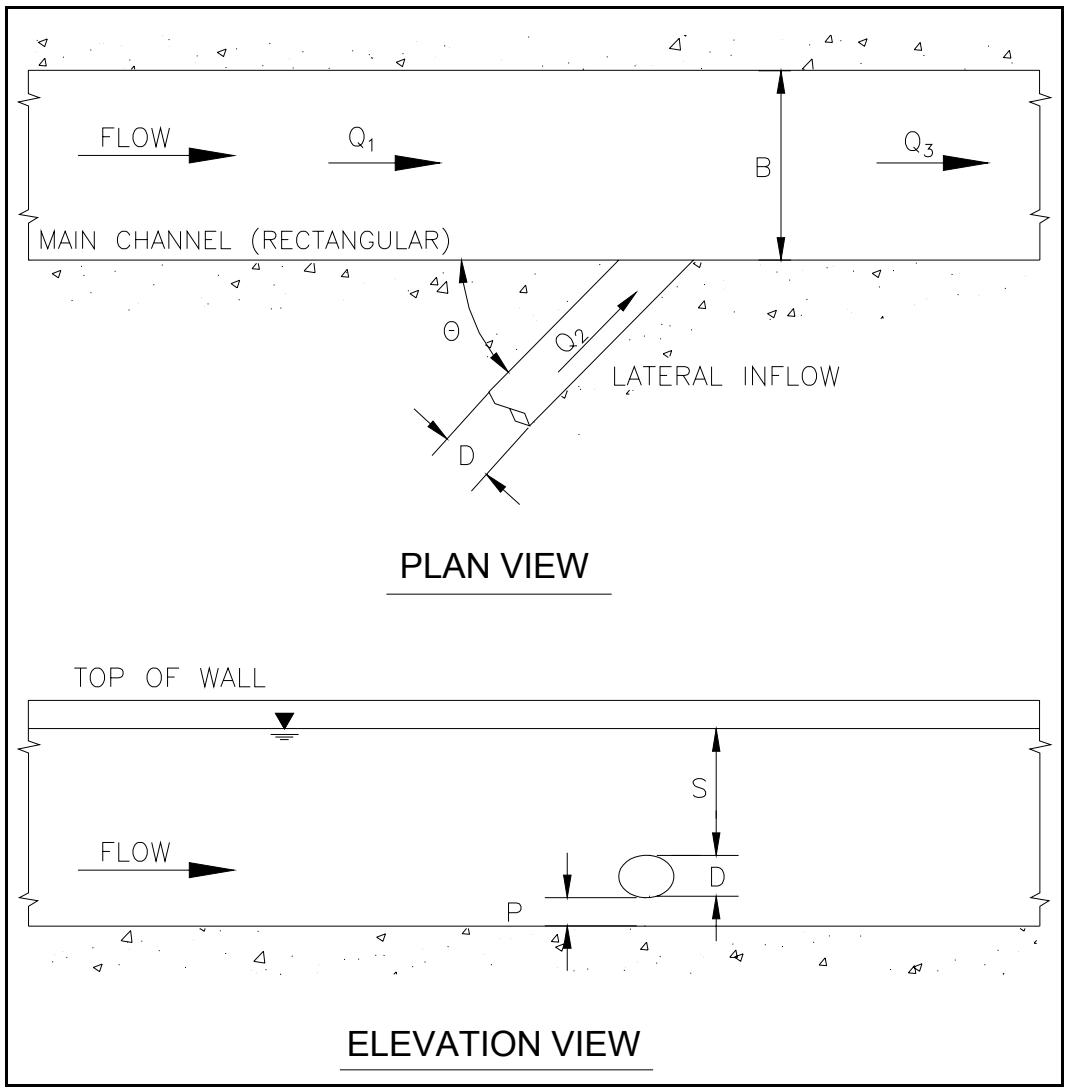

Figure 5. Layout of lateral inflow into main channel.

Even when the culvert discharge is less than 10 percent of the main channel flow, the momentum effects can produce significant bulking of the main channel flow. That is, locally, the main channel water-surface elevation can be raised by the introduction of lateral culvert flow. In some cases, the flow in the main channel may be subcritical for a short distance upstream and downstream of the lateral. Photographs of flow in high-velocity channels are provided in Figure 6. The pictures show the water surface bulking due to lateral inflow. An understanding of the flow conditions in the vicinity of laterals is essential in an economical design of these structures. Lateral inflows that intersect sidewalls at 90-degree angles provide no momentum in the main-channel alignment direction, so the flow conditions are difficult to describe analytically with one-dimensional equations.

Figure 6. Standing waves associated with lateral inflows.

The current research evaluates a modeling method to determine if it is appropriate for simulating the flow depth increases attributed to lateral inflows in rectangular high-velocity channels having fixed boundaries. Model results are validated with laboratory data of supercritical junction flow. This report presents a series of laboratory experiments followed by

numerical simulations. A two-dimensional (2D) model was applied to the supercritical flow with lateral inflow from a pressurized culvert. Model results are compared with laboratory data to evaluate the accuracy of the 2D modeling approach. Following model validation, various geometric and hydraulic conditions were studied to evaluate hydraulic conditions such as the location and magnitude of peak depths. Knowledge of these flow conditions is necessary for hydraulic design of channel walls (height and length) required to contain flows in the vicinity of laterals.

2 Theoretical Considerations

A significant volume of research has been directed toward describing flow at open channel junctions. However, only a limited number of studies have dealt with supercritical flow and cases where the side inflow is from a lateral rather than free-surface flow. Open-channel junctions of supercritical flow are briefly described in EM 1110-2-1601. The geometric layout of open-channel junctions for supercritical flow is provided in Plates B-56 and B-57 of EM 1110-2-1601 (Figures 7 and 8). Figures 9 and 10 are sketches of wave patterns and depth increases at open channel junctions as provided in Plates B-53 and B-54 of EM 1110-2-1601.

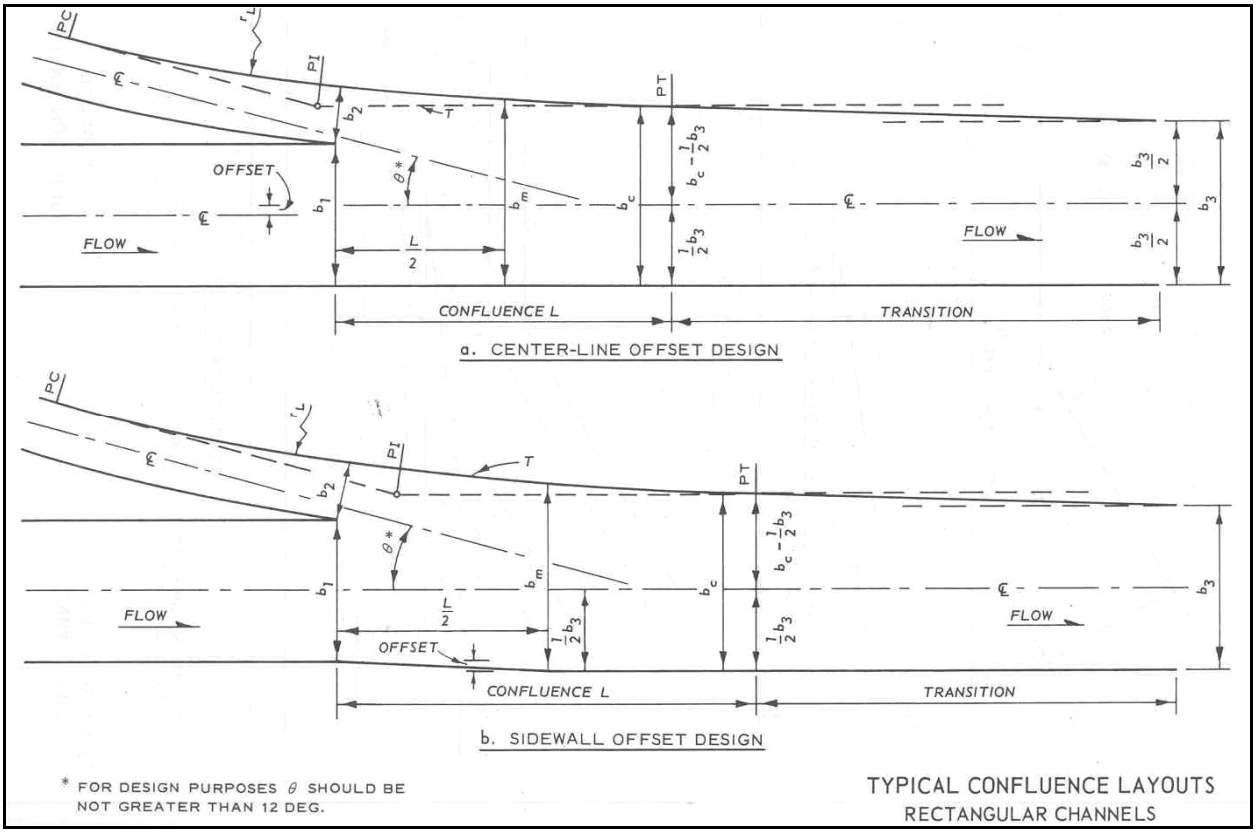

Figure 7. Plate B-56 from EM 1110-2-1601.

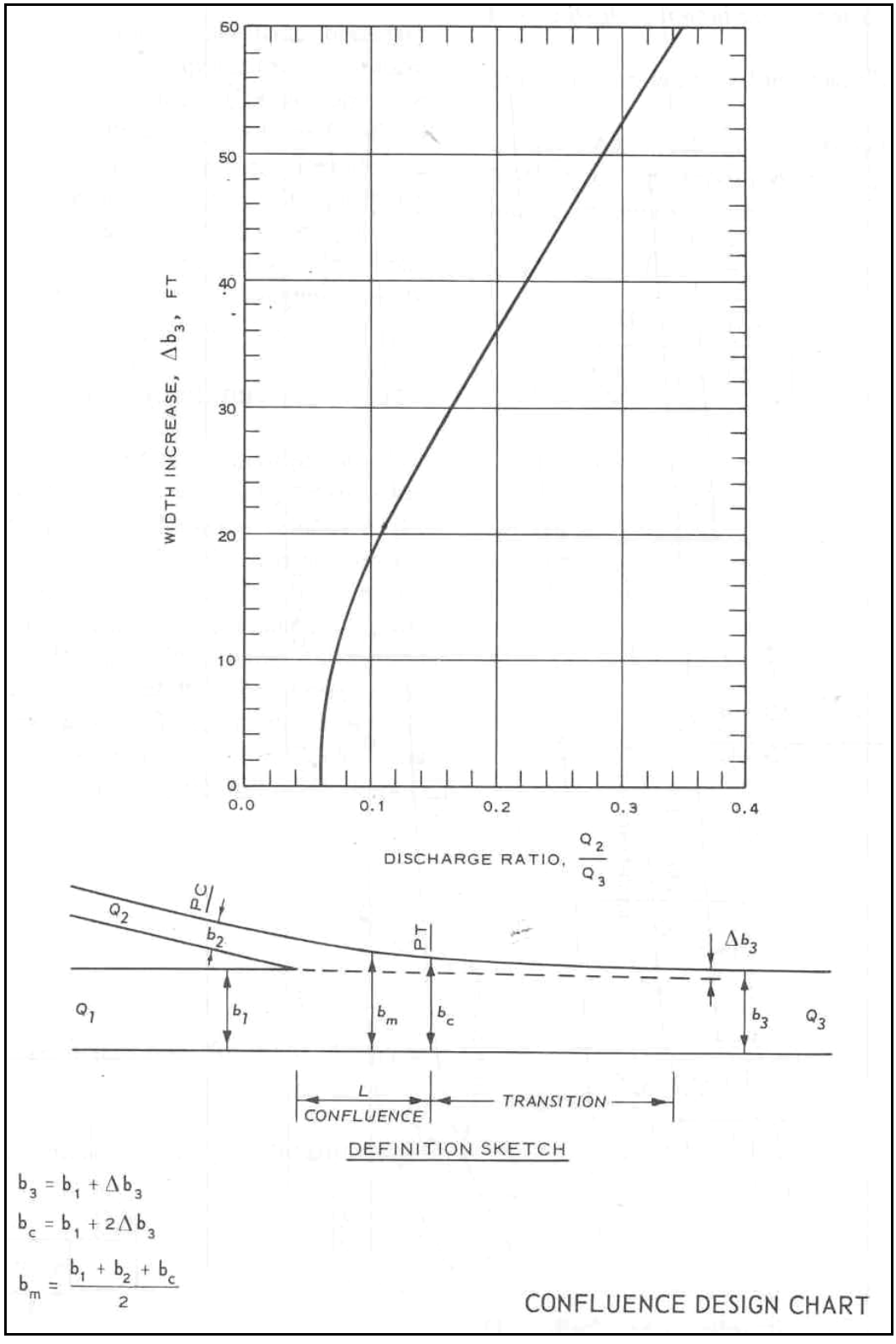

Figure 8. Plate B-57 from EM 1110-2-1601.

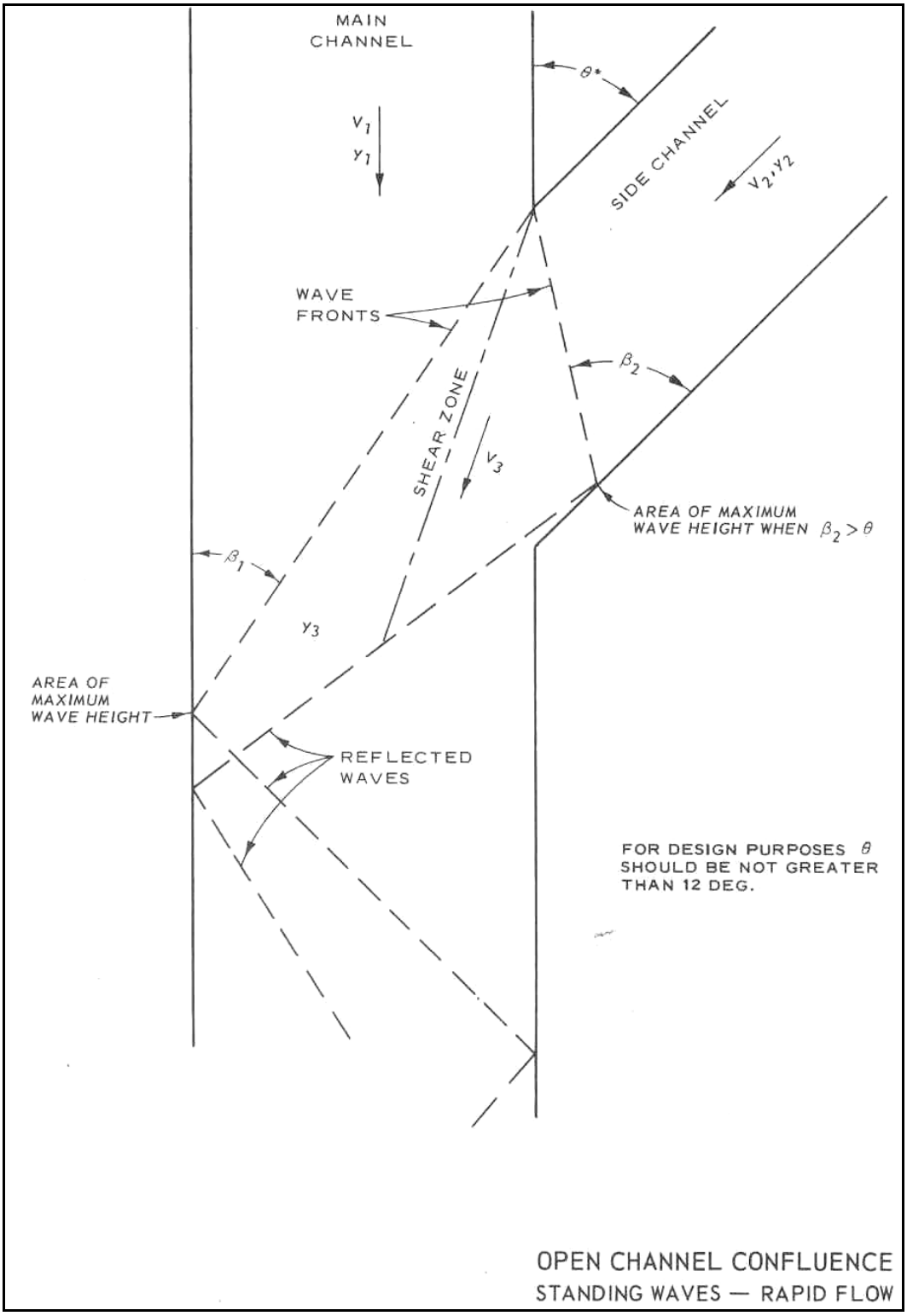

Figure 9. Plate B-53 from EM 1110-2-1601.

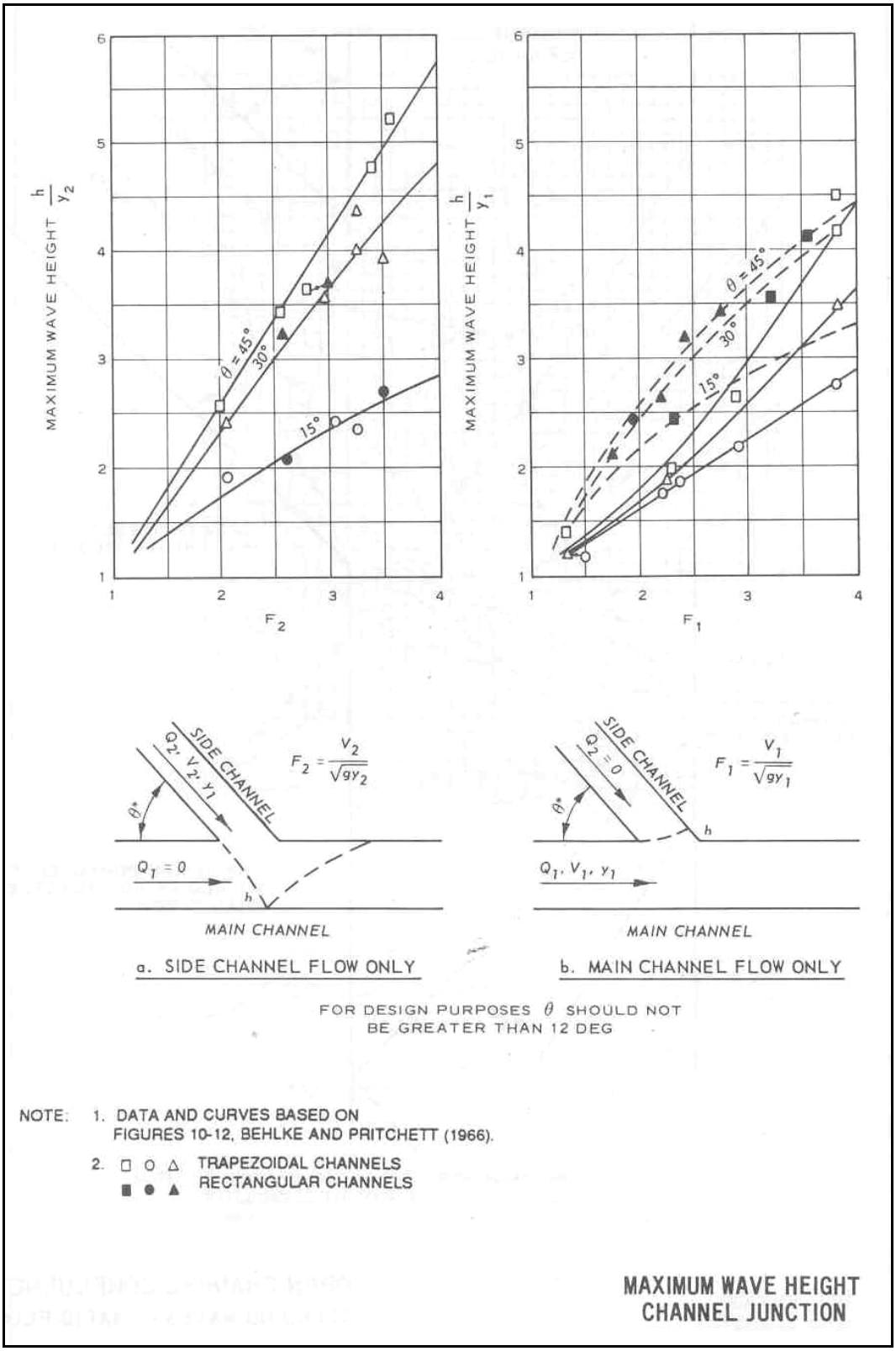

Figure 10. Plate B-54 from EM 1110-2-1601.

The Corps of Engineers' Los Angeles District has conducted the most comprehensive study of lateral designs (U.S. Army Engineer District, Los Angeles, 1960). It is not surprising that the Los Angeles District (1964) found that "the disturbance created in the channel by the side drains is directly proportional to the angle of intersection of the two flows; minimum disturbance results from parallel flows."

Conservation equations

Continuity requires that the channel flow rate downstream of the lateral is the sum of the channel discharge upstream and that of the lateral:

$$Q_1 + Q_2 = Q_3 \tag{1}$$

where Q is the discharge and the subscripts *1*, 2, and 3 identify the channel upstream of the lateral, the lateral, and the channel downstream of the lateral, respectively (Figure 5).

The energy equation written from upstream of the lateral to downstream of the lateral is:

$$\alpha_1 \frac{V_1^2}{2g} + h_1 + z_1 = \alpha_3 \frac{V_3^2}{2g} + h_3 + z_3 + \Delta E \tag{2}$$

where:

V = cross-sectional average velocity in the channel
h = cross-sectional average depth in the channel
z = invert elevation of the channel
g = gravitational acceleration
α = energy correction factor
ΔE = energy loss.

Normal flow conditions are assumed to exist immediately upstream of the lateral. A value of unity is assumed for the energy correction factor. So, given a friction factor such as Manning's roughness coefficient, n, and the bed slope, S_o, the energy location can be computed. The difference in the energy upstream and downstream is the energy loss due to the flow disturbance caused by the lateral inflow. This energy loss can be expressed in terms of the upstream velocity head with a loss coefficient, K:

$$\Delta E = K\frac{V_1^2}{2g}. \tag{3}$$

Values of K must be quantified empirically.

The linear momentum equation is developed for a rectangular channel by considering a control volume immediately inside the channel walls and just upstream and downstream of the lateral. The momentum equation is then written along the main channel direction as:

$$½\rho g b_1 h_1^2 + \delta_1 \rho \frac{Q_1^2}{b_1 h_1} + \delta_2 \rho \frac{Q_2^2}{A_2}\cos\theta = ½\rho g b_3 h_3^2 + \delta_3 \rho \frac{Q_3^2}{b_3 h_3} \tag{4}$$

where:

ρ = density of water
b = channel width
A = flow area
δ = momentum correction factor
θ = angle of the lateral.

If it is assumed that $\delta_1 = \delta_2 = \delta_3 = 1$, that the channel width is constant ($b_1 = b_3 = b$), and that the continuity equation is included, then the momentum equation can be written in terms of the downstream depth:

$$½ g b h_1^2 + \frac{Q_1^2}{b h_1} + \frac{Q_2^2}{A_2}\cos\theta = ½ g b h_3^2 + \frac{(Q_1 + Q_2)^2}{b h_3}. \tag{5}$$

Given knowledge of the upstream flow conditions and the geometric details, then this nonlinear equation for h_3 can be solved via iteration.

Governing parameters

Given the flow conditions upstream of the lateral—depth (h_1), width (b), and discharge (Q_1)—and the lateral particulars—the pipe diameter (d), submergence (S), and discharge (Q_2), then the important geometric and hydraulic parameters associated with lateral inflow are:

$$\text{Upstream Froude Number} = Fr_1 = \frac{V_1}{\sqrt{g h_1}}$$

Flow ratio = $\frac{Q_1}{Q_2}$

Width of channel to channel depth ratio = $\frac{b}{h_1}$

Pipe diameter to channel depth ratio = $\frac{d}{h_1}$

Submergence to channel depth ratio = $\frac{S}{h_1}$.

Experiments were conducted in an attempt to determine the significance of each of these parameters.

Oblique standing waves

When the flow is supercritical, oblique standing waves are generated at the lateral, and the local depth can be significantly larger than that given by Equation 5. As the supercritical flow in the main channel is disturbed by the flow issuing from the lateral, an oblique standing wave can be generated. A sketch of the wave pattern is provided in Figure 11. Even if there is no discharge from the lateral, the wall discontinuity at the lateral generates an oblique standing wave. Ippen (1951) showed that if only the disturbance point at the lateral intersection with the channel wall is considered (i.e., ignoring the flow from the lateral), then the angle is simply a function of the approaching Froude number:

$$\beta = \sin\left(\frac{1}{Fr_1}\right). \tag{6}$$

Ippen (1951) developed this relation assuming the flow is hydrostatic and that bed friction is negligible. Standing wave patterns for open-channel supercritical junction flow are provided in Plate B-53 of EM 1110-2-1601 (Figure 9).

The concern here is the peak depth, which occurs at the intersection of the standing wave and the channel wall opposite the lateral. The peak occurs at a distance downstream from the lateral, *L*, and across the channel of width, *b* (Figure 11). The peak depth occurs at the nondimensional distance from the lateral equal to *L/b*. This location is dependent on the approaching Froude number:

$$\frac{L}{b} = \sqrt{Fr^2 - 1}\ . \tag{7}$$

Actually, since the flow from the lateral alters the standing wave angle and the pressure is not hydrostatic in the vicinity of the wave, it is expected that the observed peak depth along the wall opposite the lateral will vary from the theoretical angle.

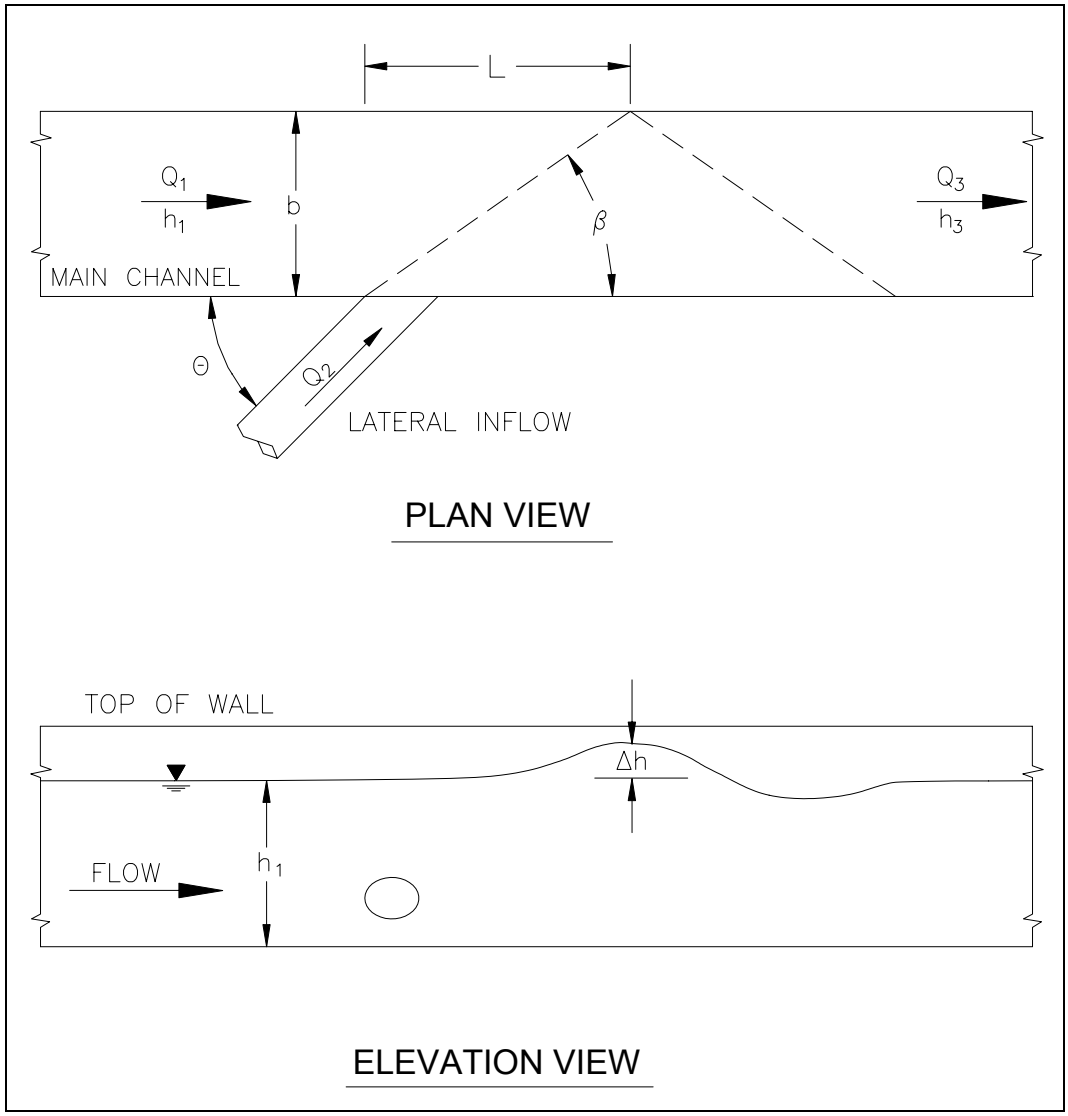

Figure 11. Wave pattern associated with lateral inflow into supercritical flow.

Choke

The choked flow condition is defined as the case where the lateral flow creates enough momentum loss in the main channel flow that a hydraulic jump is formed. This transition from supercritical flow to subcritical flow

usually occurs in an undular jump forming upstream of the lateral. The undular jump is characterized by a series of standing waves occurring over a relatively long reach of the channel. A thorough description of undular hydraulic jumps in rectangular channels is given by Ohtsu et al. (2003). The flow depths of the resulting subcritical flow are significantly larger than normal flow depths. Both the required wall height and wall length definitely increase for a choked flow condition.

3 Physical Model

The flume constructed for this study was of rectangular cross-sectional shape. The walls and invert were made of smooth plastic-coated plywood having a Manning's *n* of 0.01. The flume was 2.0 ft (0.610 m) wide by more than 40 ft (12 m) long. The bed slope was 0.0095, providing super-critical flow under normal flow conditions. Lateral flow was introduced to the channel by a 2-in.- (5-cm-) diameter PVC pipe with invert that was 0.04 ft (1 cm) above the channel invert. The pipe was angled at 90 degrees to the right sidewall (looking downstream). A metered water discharge was supplied to the flume (main channel upstream of the lateral) by a circulating system. The total flow including the lateral inflow was measured below the end of the flume using a v-notch weir. The difference was known to be the lateral discharge. Depths were measured using a point gage. The laboratory data were measured in U.S. customary units, and the results are presented in such units.

Five flow conditions were documented in the physical model. The flow conditions evaluated are shown in Table 1.

Table 1. Flow conditions evaluated in the physical model and the HIVEL2D model.

Test Number	Q_1, cfs (cms)	Froude Number at Normal Flow	Q_2, cfs (cms)	Discharge Ratio, Q_2/Q_1
LV 1	1.03 (0.314)	1.70	0.050 (0.015)	5%
LV 2	1.03 (0.314)	1.70	0.105 (0.032)	10%
LV 3	1.51 (0.460)	1.71	0.150 (0.046)	10%
LV 4	1.75 (0.533)	1.74	0.175 (0.053)	10%
LV 5	0.52 (0.159)	1.63	0.050 (0.015)	10%

In model operation, for test number LV 4, for example, the main channel inflow was set to 1.75 cfs (0.533 cms). The lateral inflow was 10 percent of the main channel, or 0.175 cfs (0.053 cms). The normal depth of 0.20 ft (6.1 cm) was set at the upper end of the flume. At normal flow conditions the velocity is 4.40 fps (1.34 mps) and the Froude number is 1.74.

Photographs of the flow conditions in the laboratory flume for each of the tests are provided in Figures 12–17. The lateral flow creates a choked condition whereby an undular jump is formed upstream of the junction.

Figure 12. Flow conditions with main channel discharge = 1.03 cfs (0.314 cms), lateral discharge = 0.05 cfs (0.015 cms) (looking downstream).

This deeper flow is a local phenomenon in that the flow accelerates back to supercritical downstream of the junction.

Flow depths were measured at sufficient resolution to construct depth contour plots. The physical model data are provided in the next chapter (Chapter 4). Chapter 4 includes comparisons of observed and computed depths for the five test conditions documented in the physical model.

Figure 13. Flow conditions with main channel discharge = 1.03 cfs (0.314 cms), lateral discharge = 0.105 cfs (0.032 cms) (looking downstream).

Figure 14. Flow conditions with main channel discharge = 1.51 cfs (0.460 cms), lateral discharge = 0.15 cfs (0.046 cms) (looking downstream).

Figure 15. Flow conditions with main channel discharge = 1.75 cfs (0.533 cms), lateral discharge = 0.175 cfs (0.053 cms) (looking downstream).

Figure 16. Flow conditions with main channel discharge = 1.75 cfs (0.533 cms), lateral discharge = 0.175 cfs (0.053 cms) (looking upstream).

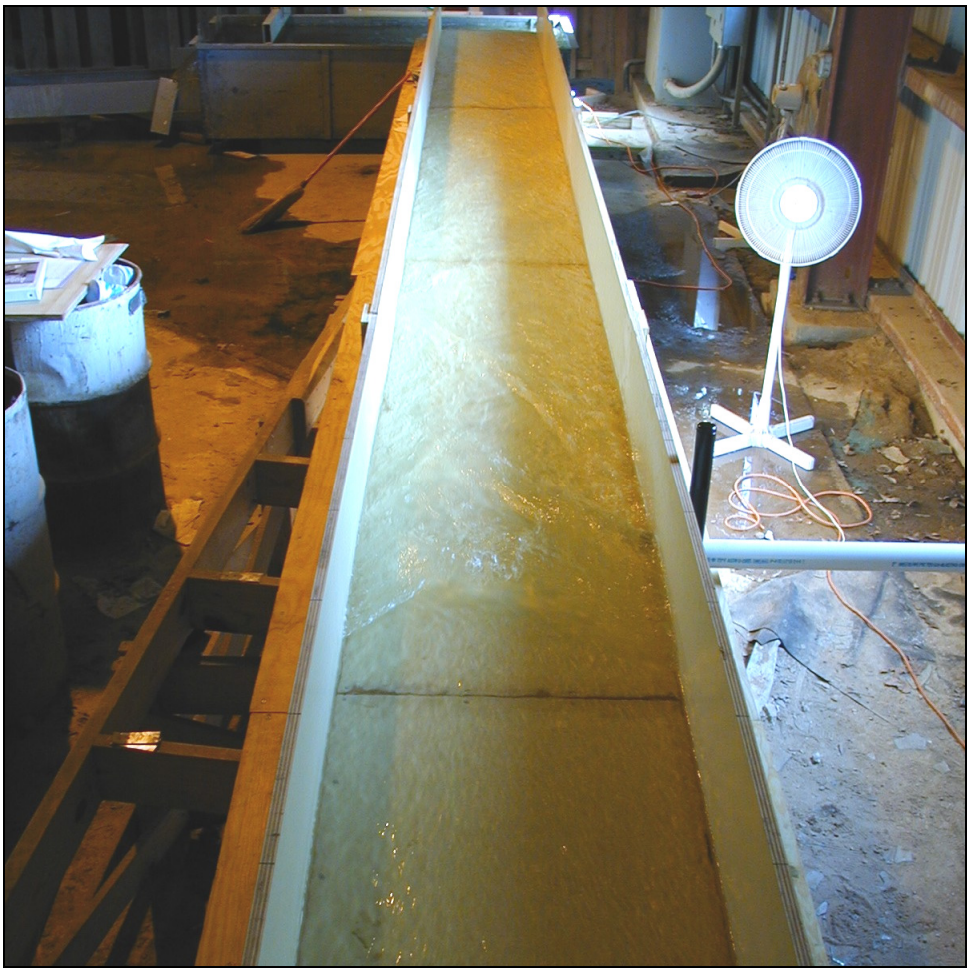

Figure 17. Flow conditions with main channel discharge = 0.52 cfs (0.159 cms), lateral discharge = 0.05 cfs (0.016 cms) (looking downstream).

4 Two-Dimensional Numerical Model

Although the lateral flow entering the channel is from a submerged pipe flowing under pressure, a two-dimensional (2D) model was tested to see how well it could simulate the flows documented in the laboratory flume. Of course, several liberties in boundary conditions at the pipe outlet had to be made because the 2D model is a depth-averaged, free-surface representation of the real system. However, the momentum and additional mass create the disturbances in the main channel, the primary one of which is flow choking.

The shallow-water (or long-wave) equations are a result of the vertical integration of the equations of mass and momentum conservation for incompressible flow under the hydrostatic pressure assumption. The flow depth (h), the x-component of velocity (u), and the y-component of velocity (v) define the dependent variables of the fluid motion. If the fluid pressure at the surface is taken as zero and the free-surface stresses are neglected, the shallow-water equations are given as:

$$\frac{\partial \mathbf{U}}{\partial t} + \frac{\partial \mathbf{F}}{\partial x} + \frac{\partial \mathbf{G}}{\partial y} + \mathbf{H} = 0 \tag{8}$$

where:

$$\mathbf{U} = \begin{Bmatrix} h \\ uh \\ vh \end{Bmatrix} \tag{9}$$

$$\mathbf{F} = \begin{Bmatrix} hu \\ hu^2 + \frac{1}{2} gh^2 - h\frac{\sigma_{xx}}{\rho} \\ huv - h\frac{\sigma_{yx}}{\rho} \end{Bmatrix} \tag{10}$$

$$\mathbf{G} = \begin{Bmatrix} hv \\ huv - h\dfrac{\sigma_{xy}}{\rho} \\ hv^2 + \frac{1}{2}gh^2 - h\dfrac{\sigma_{yy}}{\rho} \end{Bmatrix} \tag{11}$$

$$\mathbf{H} = \begin{Bmatrix} 0 \\ gh\dfrac{\partial z_b}{\partial x} + n^2 g \dfrac{u\sqrt{u^2+v^2}}{C_0 h^{4/3}} \\ gh\dfrac{\partial z_b}{\partial y} + n^2 g \dfrac{v\sqrt{u^2+v^2}}{C_0 h^{4/3}} \end{Bmatrix} \tag{12}$$

where:

z_b = bed elevation
n = Manning's roughness coefficient
C_o = a dimensional constant (C_o = 1 for SI units and 2.208 for non SI units)
σ = Reynolds stresses due to turbulence, where the first subscript indicates the direction and the second indicates the face on which the stress acts.

The equations are discretized using the finite element method in which u, v, and h are represented as linear polynomials on each element. The finite element scheme is an SUPG scheme similar to that reported in Berger and Stockstill (1995). The computer programs are HIVEL2D and ADH. Each code solves the shallow-water equations in essentially the same manner. Early runs for comparing simulation results with laboratory observations employed HIVEL2D. However, ADH has more features such as mesh adaption and therefore is presently the code of choice.

The primary objective of a flood-control channel is containing flood flows. So, the primary objective in modeling these channels is accurately computing the depth of flow throughout the flow domain. Comparisons of laboratory data with model results consist of evaluating the model's ability to reproduce the water-surface contours observed in the laboratory flume.

Depths measured in the flume are compared with the 2D model results. The comparisons are plotted as depth contours in Figures 18–22. The shallow-water model results shown in Figures 20–22 indicate that the model is not capable of capturing undular jumps. This is because the model ignores vertical inertia. Also, the hydrostatic pressure assumption in the shallow-water equations produces small errors in the wave angle. This is discussed further in the next chapter.

The 2D numerical model, with its limitations, provides crosswise variation of depth and velocity, unlike analytical descriptions and one-dimensional models that neglect lateral variations. Also, analytical descriptions generally ignore boundary shear stresses, which are accounted for in the numerical model. The only limitation is that vertical accelerations are neglected, which requires that the pressure distribution be hydrostatic. The numerical model is capable of simulating the oblique standing wave generated by the lateral flow. The model computes peak depth with reasonable accuracy, and although undular hydraulic jumps are missed, the choke condition is reproduced. The model not only captures the oblique standing wave and choke condition, but it also reproduces the accelerations as the flow downstream of the lateral returns to the normal depth. Although the results presented in this study are steady-state conditions, the model is capable of modeling unsteady flow. So, hydrographs of various timings can be simulated for the channel and the lateral. Most importantly, the numerical model is capable of identifying unsatisfactory flow conditions and pointing to the need for hydraulic design improvements.

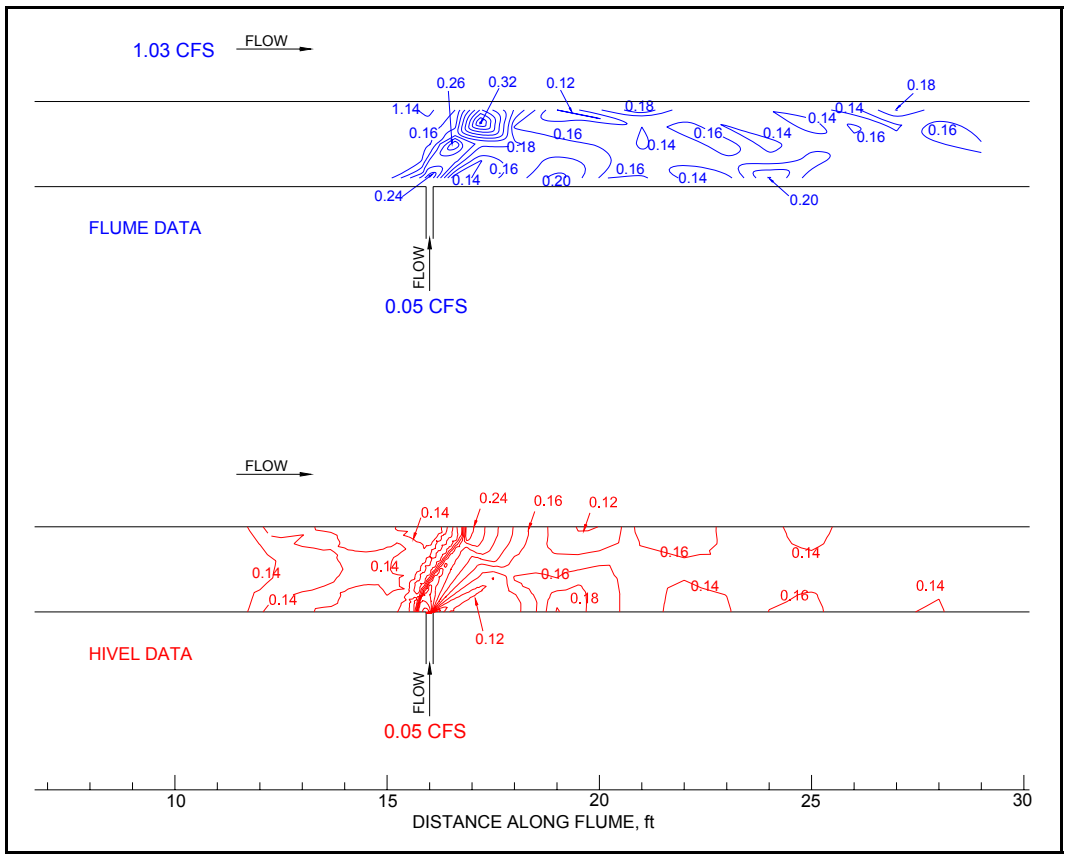

Figure 18. Observed (flume data) and computed (HIVEL2D) depth contours for main channel discharge = 1.03 cfs (0.314 cms), lateral discharge = 0.05 cfs (0.015 cms).

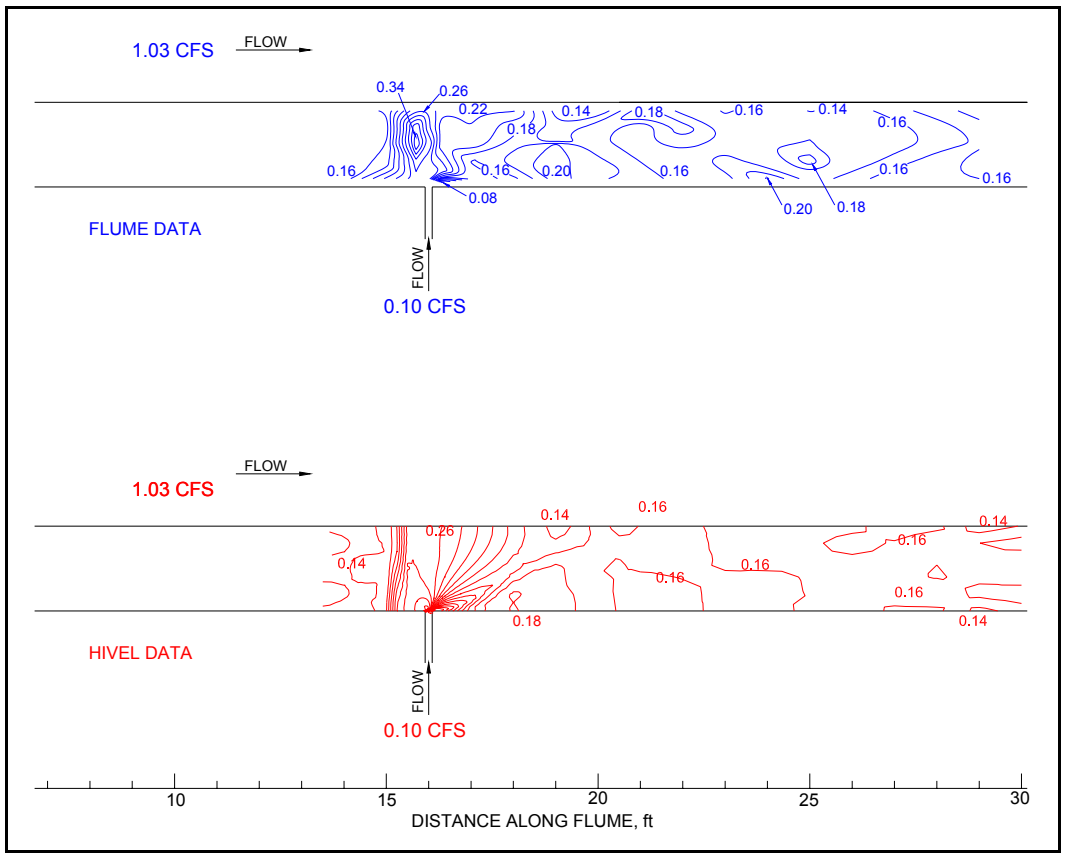

Figure 19. Observed (flume data) and computed (HIVEL2D) depth contours for main channel discharge = 1.03 cfs (0.314 cms), lateral discharge = 0.105 cfs (0.032 cms).

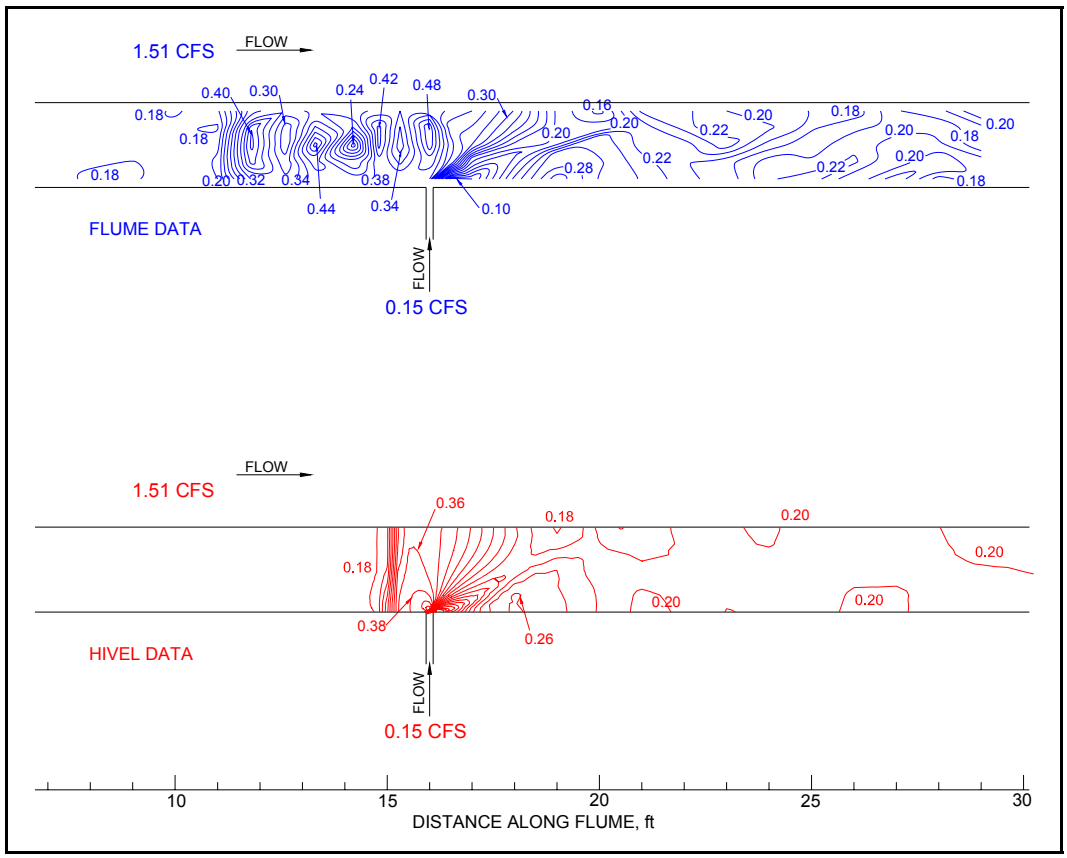

Figure 20. Observed (flume data) and computed (HIVEL2D) depth contours for main channel discharge = 1.51 cfs (0.460 cms), lateral discharge = 0.15 cfs (0.046 cms).

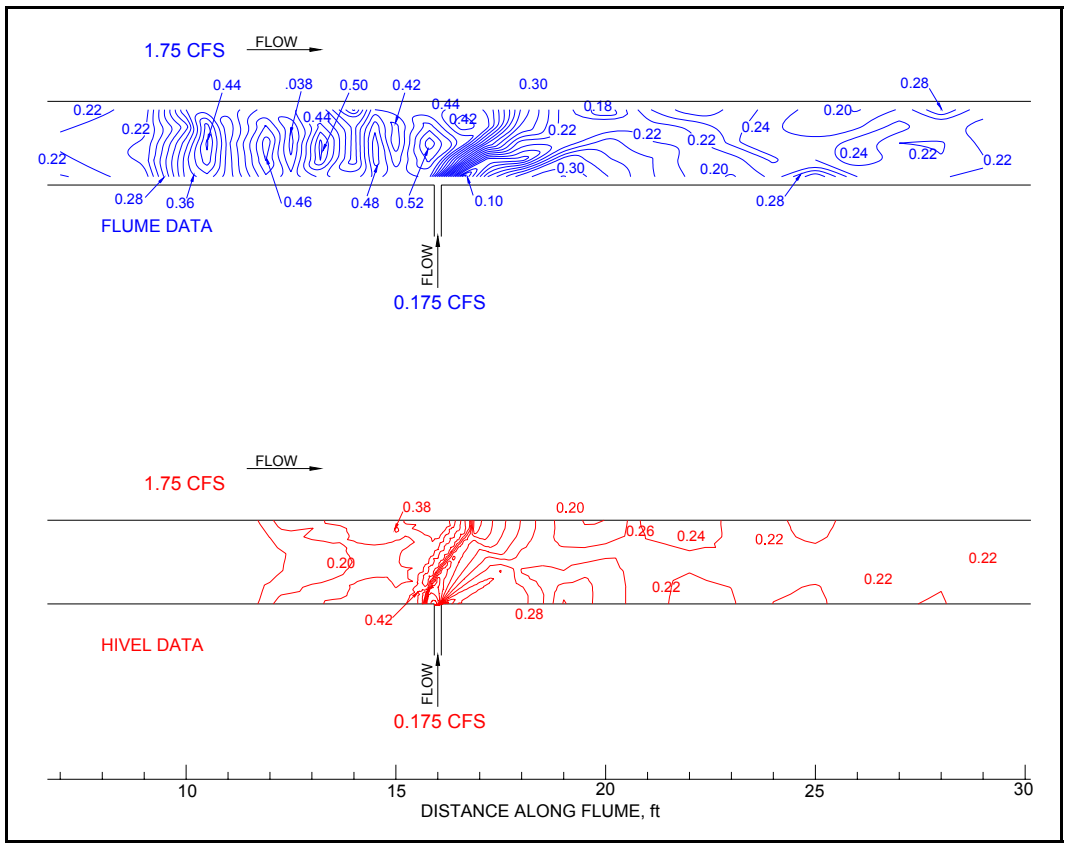

Figure 21. Observed (flume data) and computed (HIVEL2D) depth contours for main channel discharge = 1.75 cfs (0.533 cms), lateral discharge = 0.175 cfs (0.053 cms).

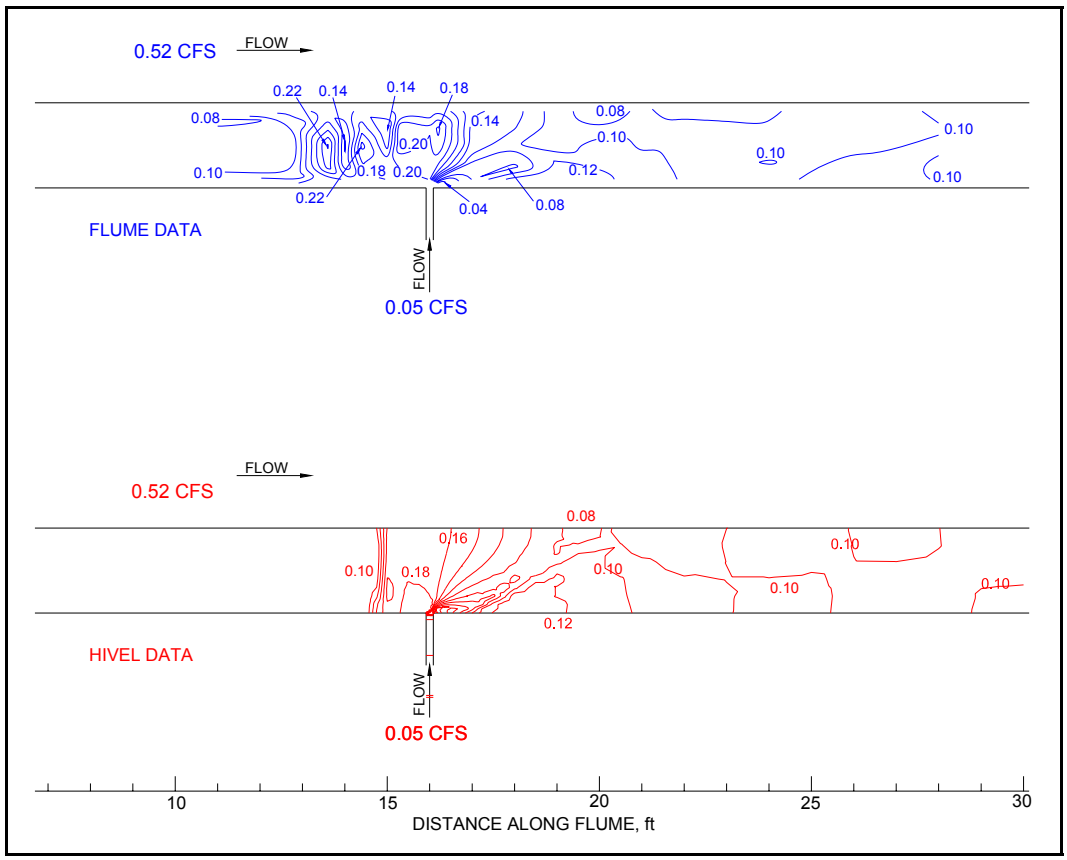

Figure 22. Observed (flume data) and computed (HIVEL2D) depth contours for main channel discharge = 0.52 cfs (0.159 cms), lateral discharge = 0.05 cfs (0.016 cms).

5 Results

This chapter examines the influence of the parameters listed in Chapter 2. The information is obtained from the physical model and supplemented with the numerical model results. Additional data were obtained from the U.S. Army Engineer District, Los Angeles (1960) report and a physical model study of the Hoosic River flood control channel (U.S. Army Engineer Waterways Experiment Station 1962). These physical models provide only a few data points, but as mentioned earlier, data from studies of lateral inflows are quite limited. The results of various physical models are supplemented with the numerical model results to quantify the local depth increases. The numerical model simulated various channel flow rates, lateral discharge to main-channel discharge ratios, and the lateral angle. These flow conditions are listed in Table 2.

The results of the simulation of the hydraulic and geometric parameters listed in Table 2 are shown on Figures 23–49. Each of these figures provides a picture of the computed water surface and plots water-surface contours and profiles along each wall.

Energy loss

The computer simulations were used to quantify the loss coefficient for various angles and discharge ratios. A graph showing the variation of K for lateral discharge to main-channel discharge ratios of 0.01, 0.05, and 0.10 and lateral angles of 30° and 60° is shown in Figure 50. Laterals at angles of 90° choked the flow, so energy losses were difficult to establish since the resulting hydraulic jump often migrated to the upstream model limit. Design criteria require that side inflow rates greater than 10 percent of the main channel flow should be introduced as a confluence design rather than as a lateral. The results suggest that a lateral angle of 60° results in less head loss than an angle of 30°. This apparent discrepancy is attributed to the fact that the energy supplied to the system by the lateral was ignored in the definition of the loss coefficient, K. In general, Figure 50 indicates that a loss coefficient of 0.7 is a reasonable estimate for computation of head loss for the conditions examined.

Table 2. Flow conditions evaluated in the ADH numerical model.

Test	Q_1 (cms)	Q_2 (cms)	Q_2/Q_1 (percent)	Lateral Angle (degrees)	Upstream	
					Normal Depth (m)	Froude Number
1	110	1.10	1	30	2.05	1.5
2	110	5.50	5	30	2.05	1.5
3	110	11.00	10	30	2.05	1.5
4	195	1.95	1	30	3.08	1.4
5	195	9.75	5	30	3.08	1.4
6	195	19.50	10	30	3.08	1.4
7	320	3.20	1	30	4.46	1.4
8	320	16.00	5	30	4.46	1.4
9	320	32.00	10	30	4.46	1.4
10	110	1.10	1	60	2.05	1.5
11	110	5.50	5	60	2.05	1.5
12	110	11.00	10	60	2.05	1.5
13	195	1.95	1	60	3.08	1.4
14	195	9.75	5	60	3.08	1.4
15	195	19.50	10	60	3.08	1.4
16	320	3.20	1	60	4.46	1.4
17	320	16.00	5	60	4.46	1.4
18	320	32.00	10	60	4.46	1.4
19	110	1.10	1	90	2.05	1.5
20	110	5.50	5	90	2.05	1.5
21	110	11.00	10	90	2.05	1.5
22	195	1.95	1	90	3.08	1.4
23	195	9.75	5	90	3.08	1.4
24	195	19.50	10	90	3.08	1.4
25	320	3.20	1	90	4.46	1.4
26	320	16.00	5	90	4.46	1.4
27	320	32.00	10	90	4.46	1.4

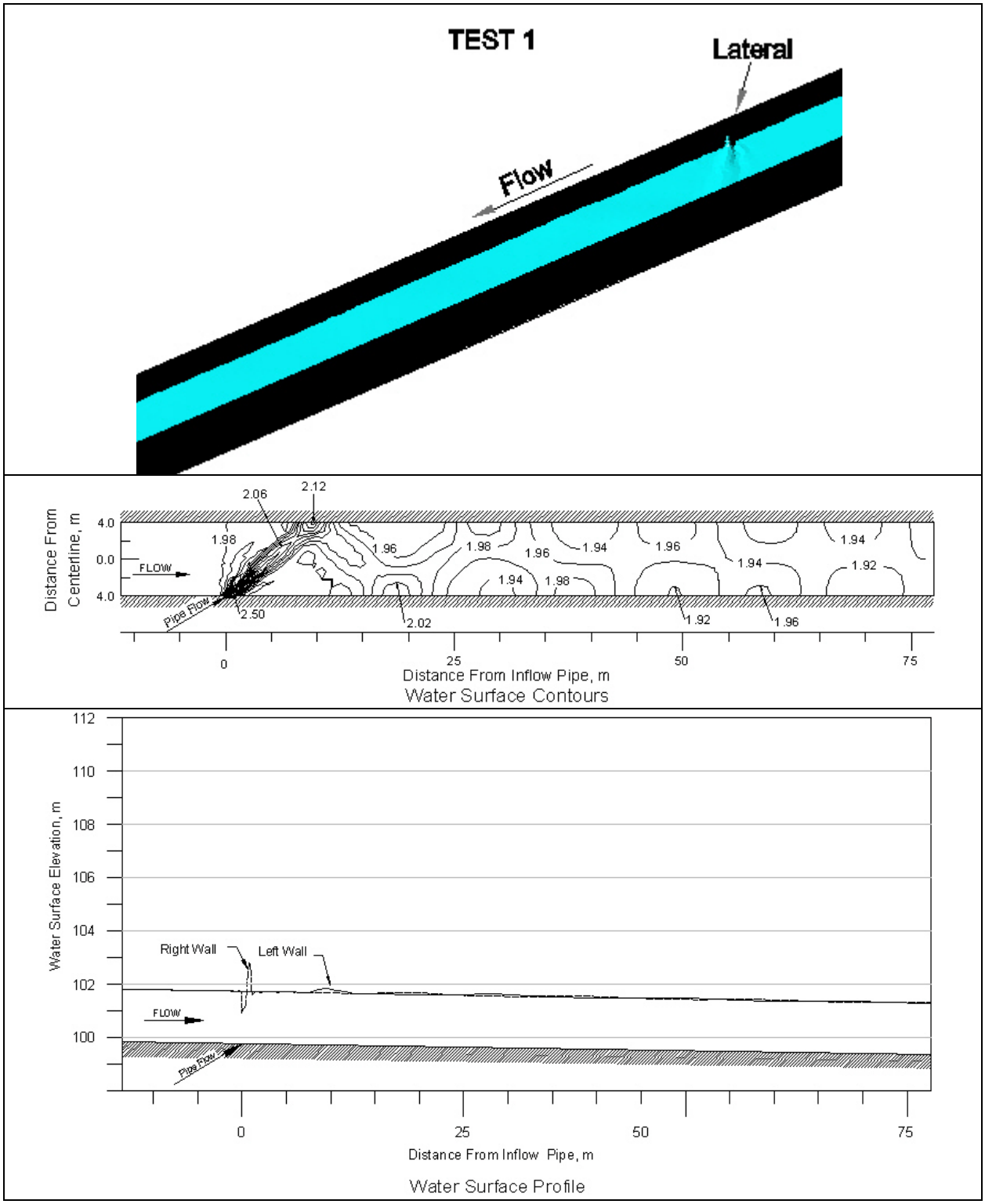

Figure 23. 2D MODEL results for Test 1.

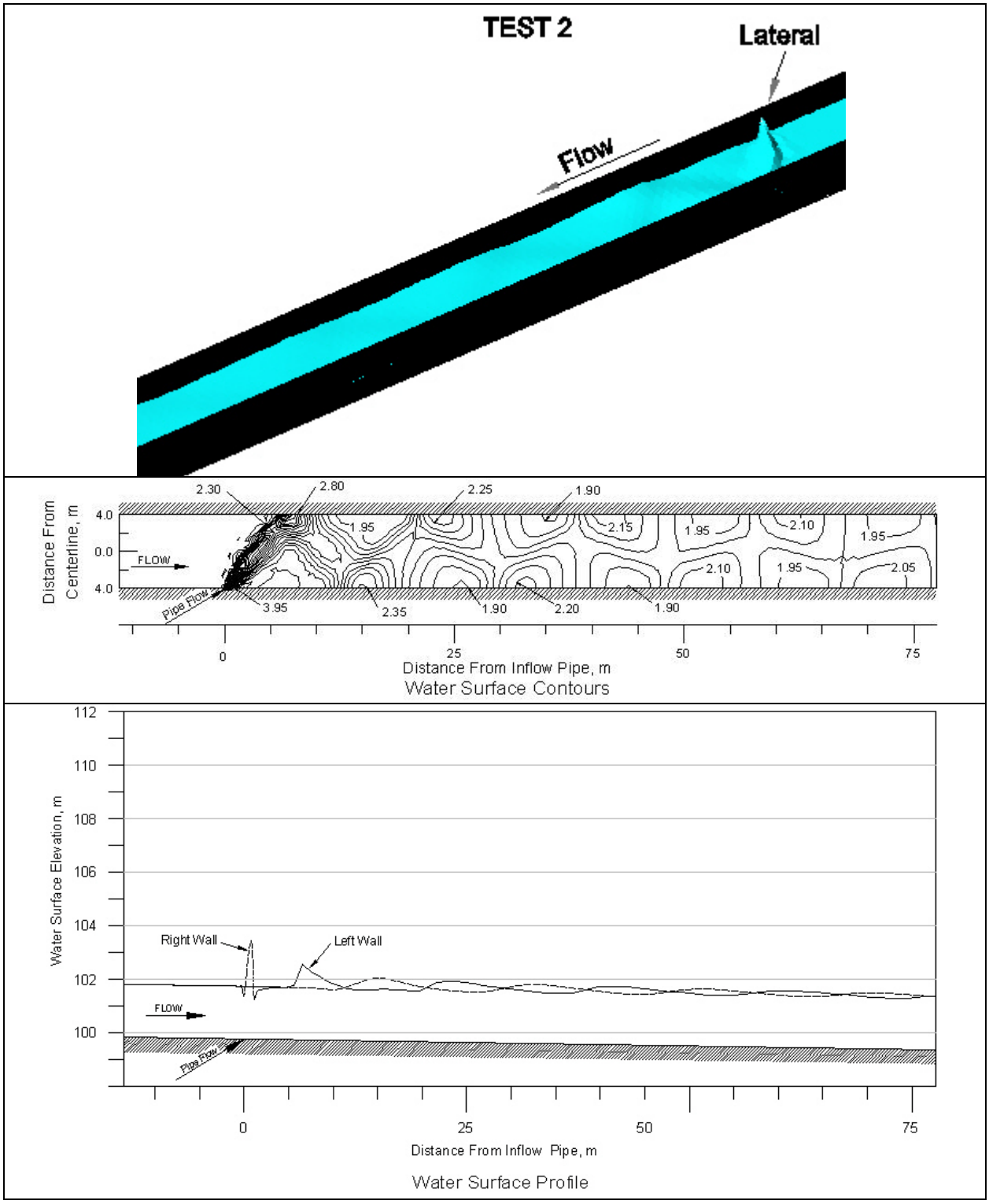

Figure 24. 2D MODEL results for Test 2.

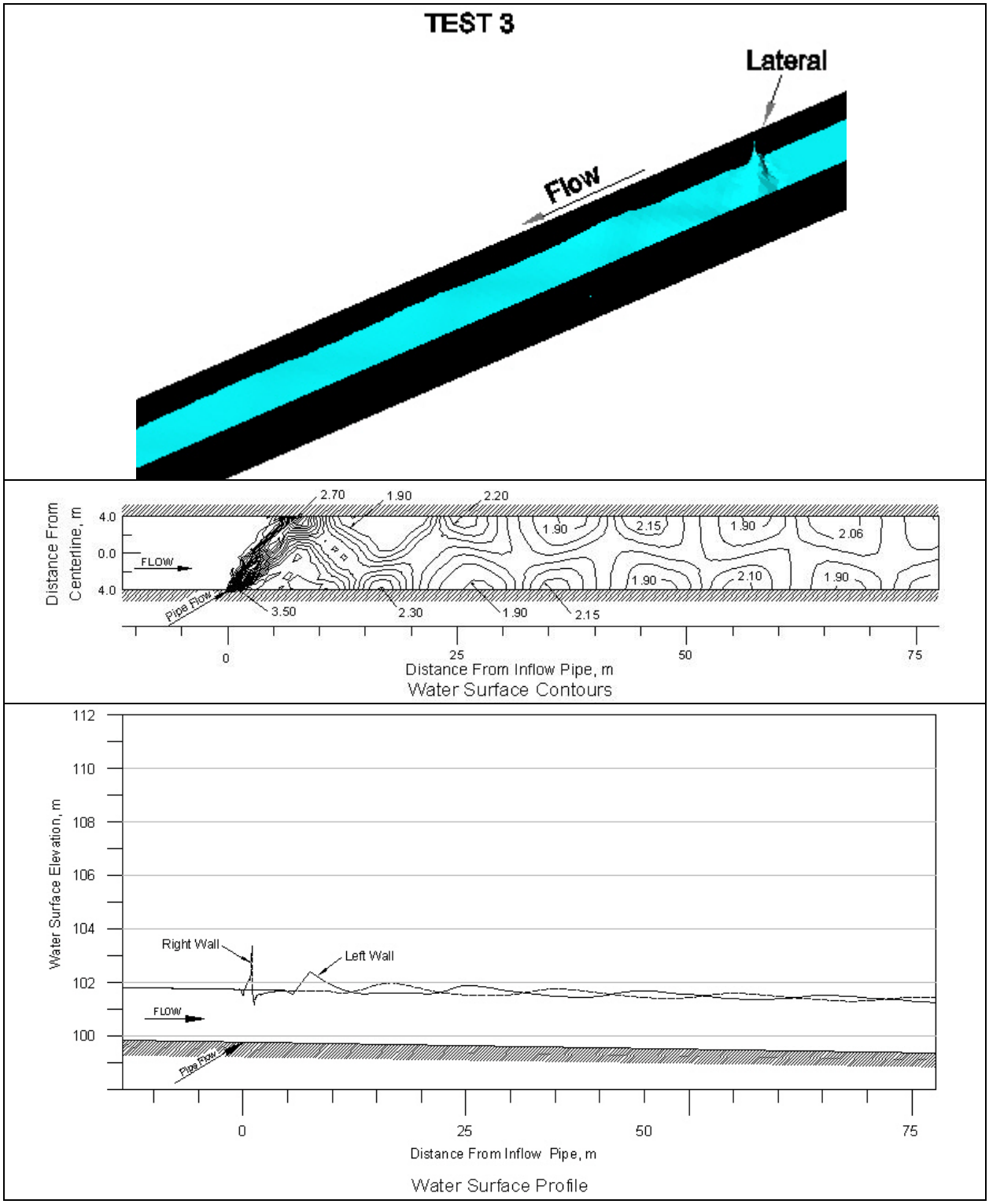

Figure 25. 2D MODEL results for Test 3.

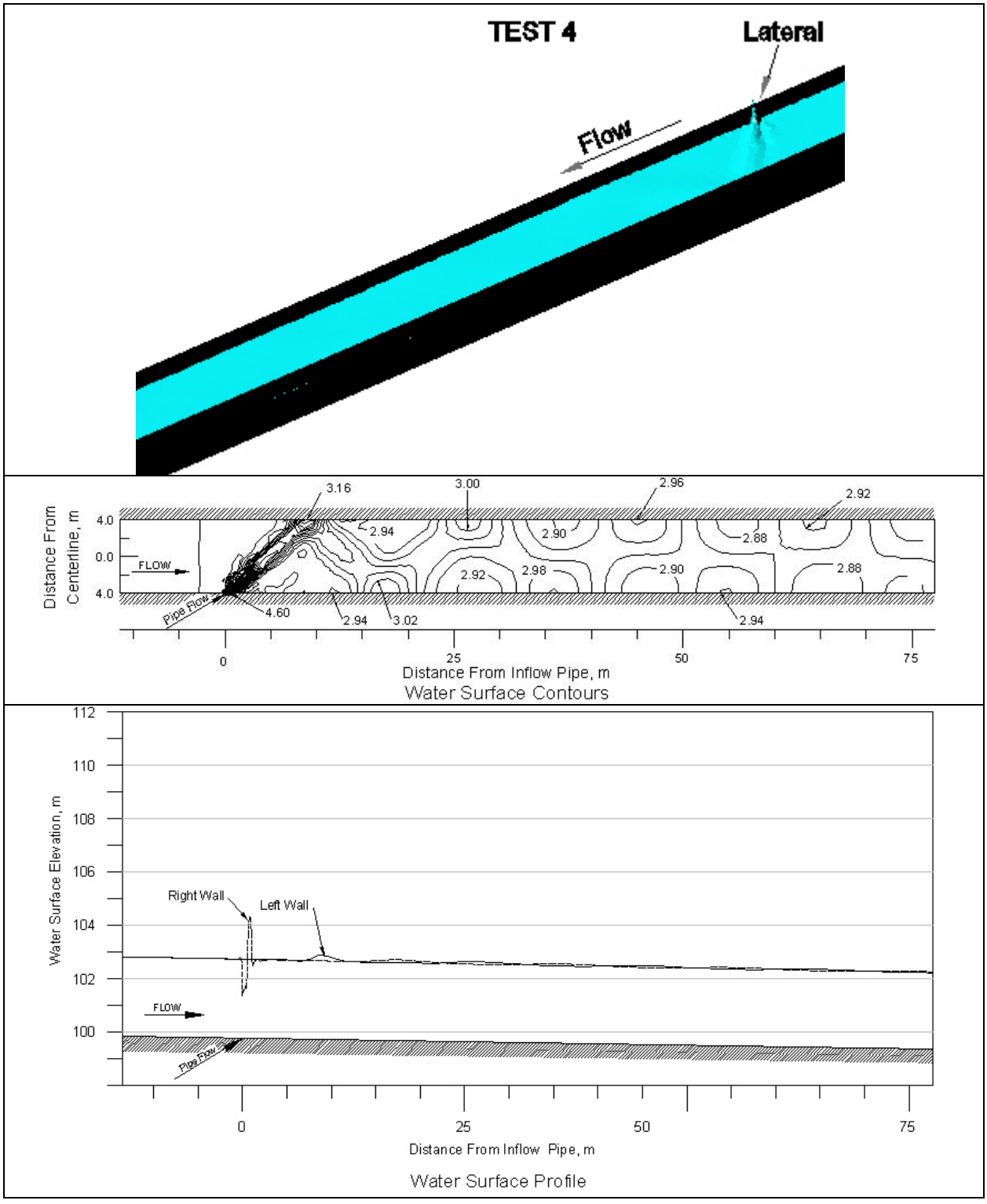

Figure 26. 2D MODEL results for Test 4.

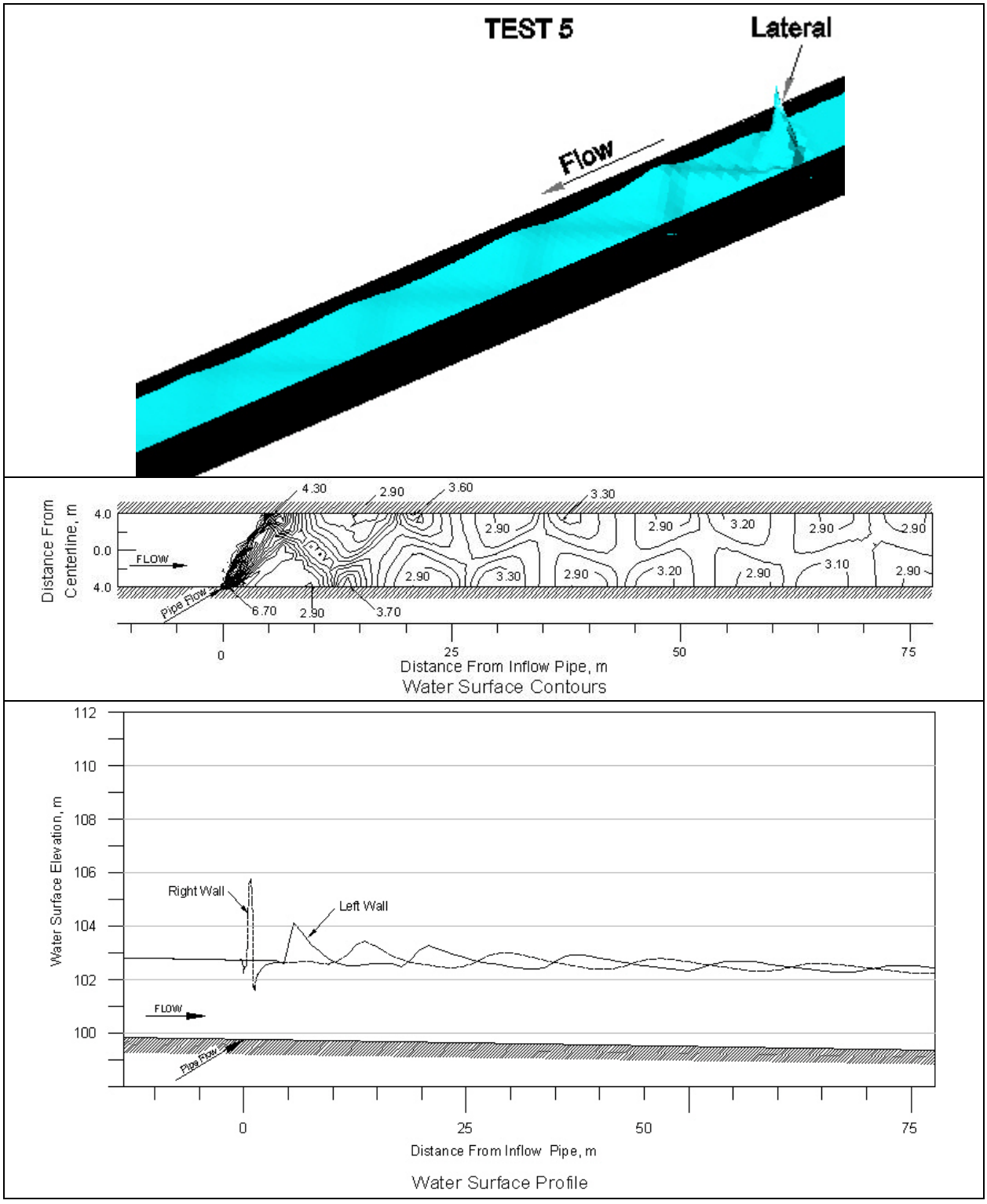

Figure 27. 2D MODEL results for Test 5.

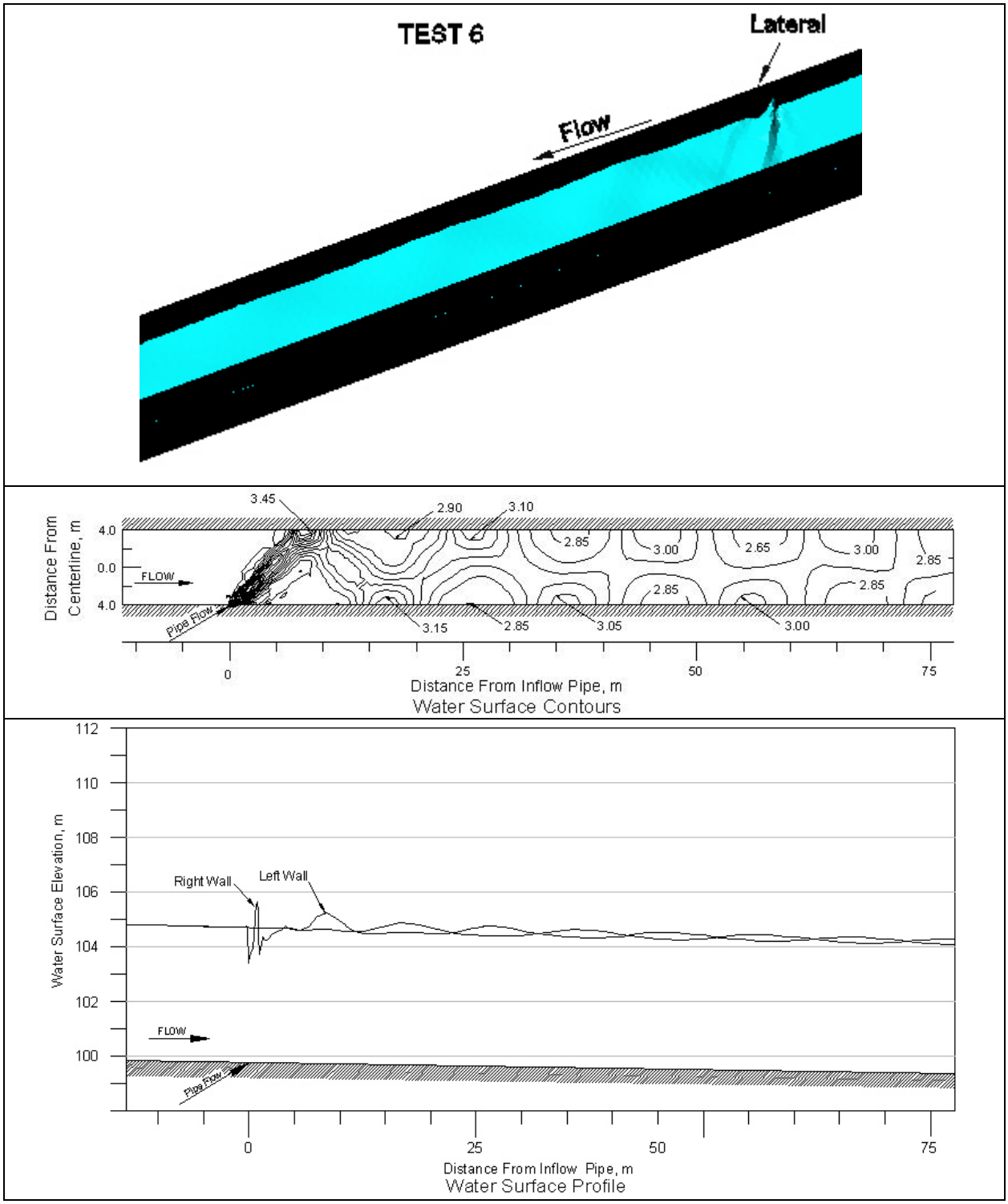

Figure 28. 2D MODEL results for Test 6.

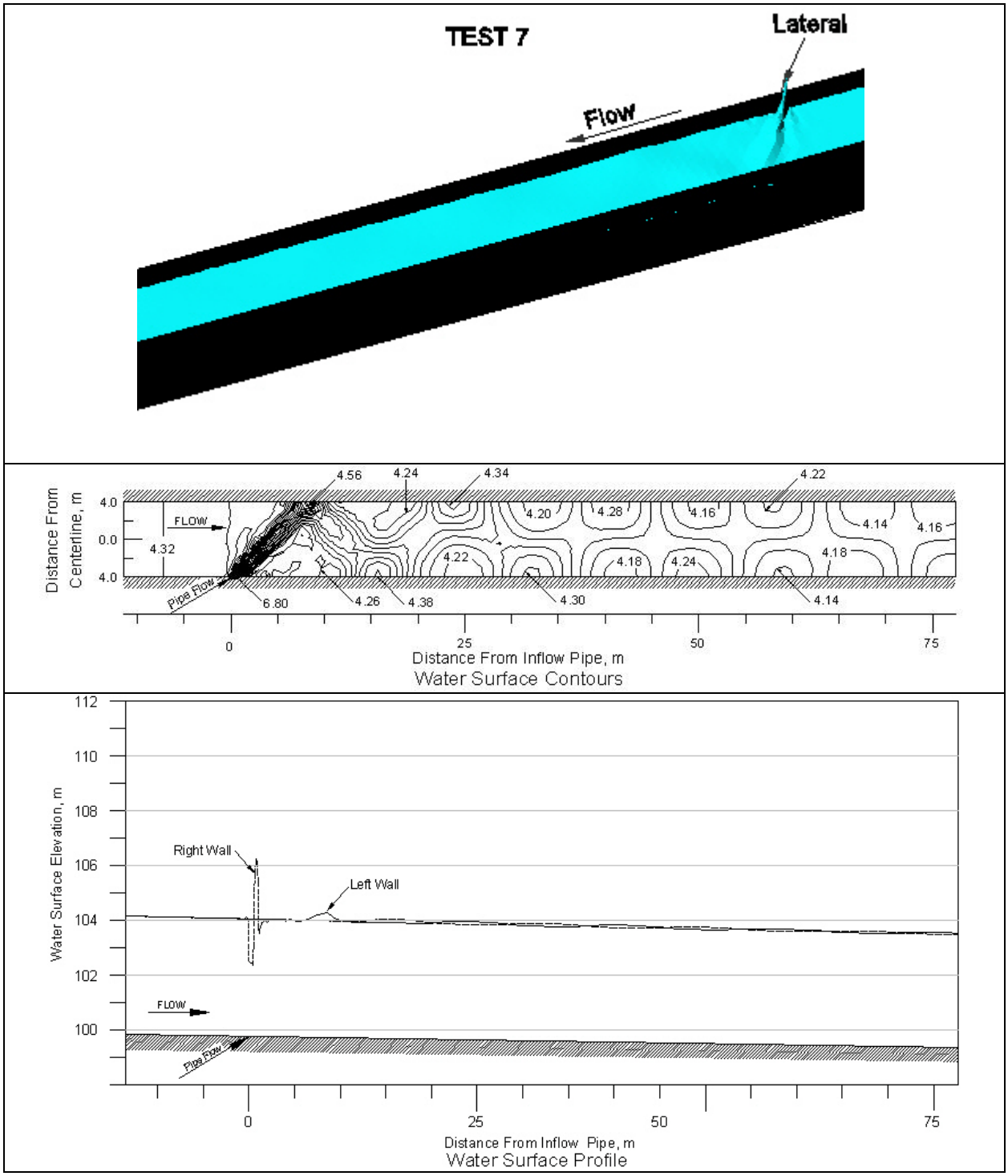

Figure 29. 2D MODEL results for Test 7.

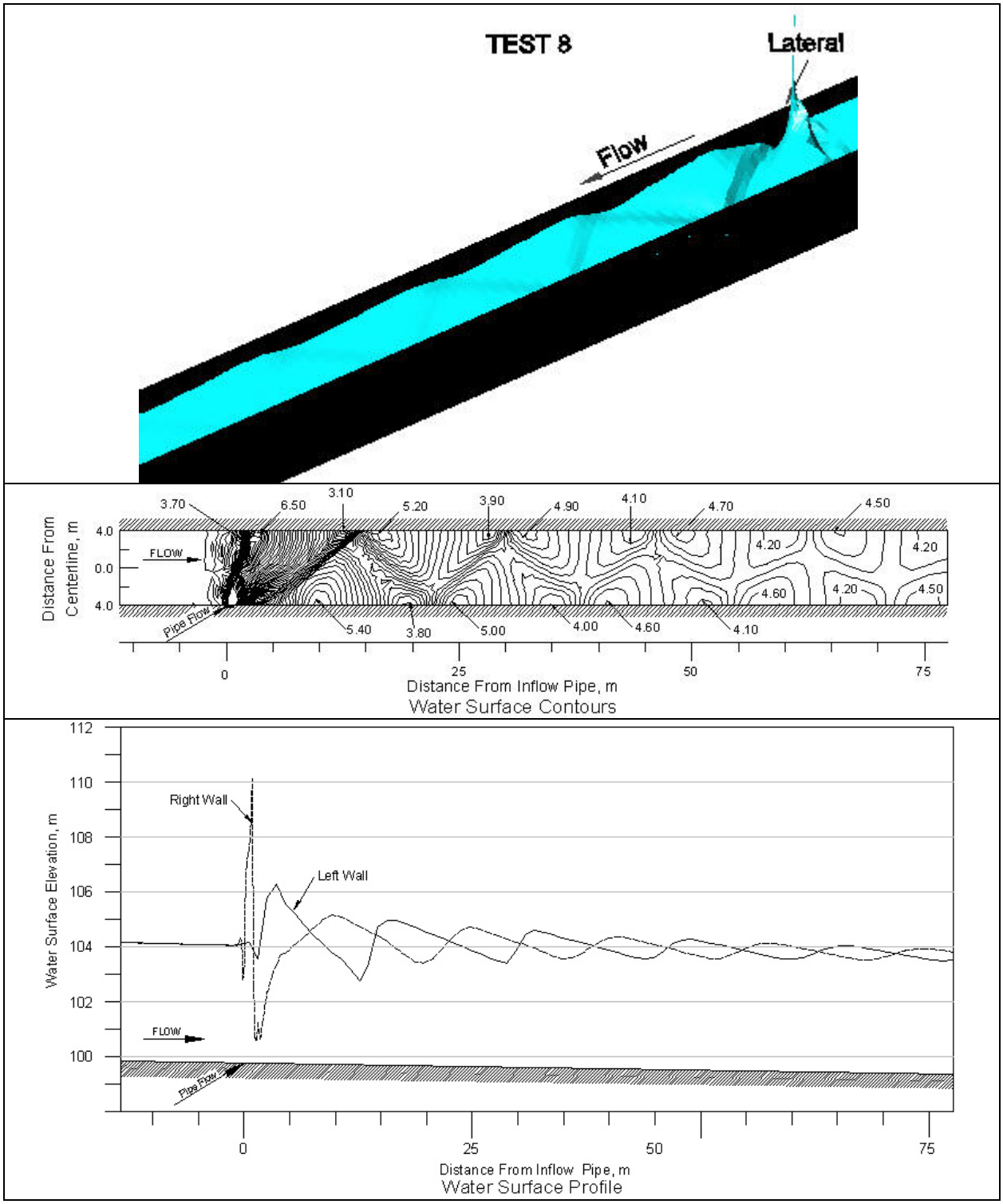

Figure 30. 2D MODEL results for Test 8.

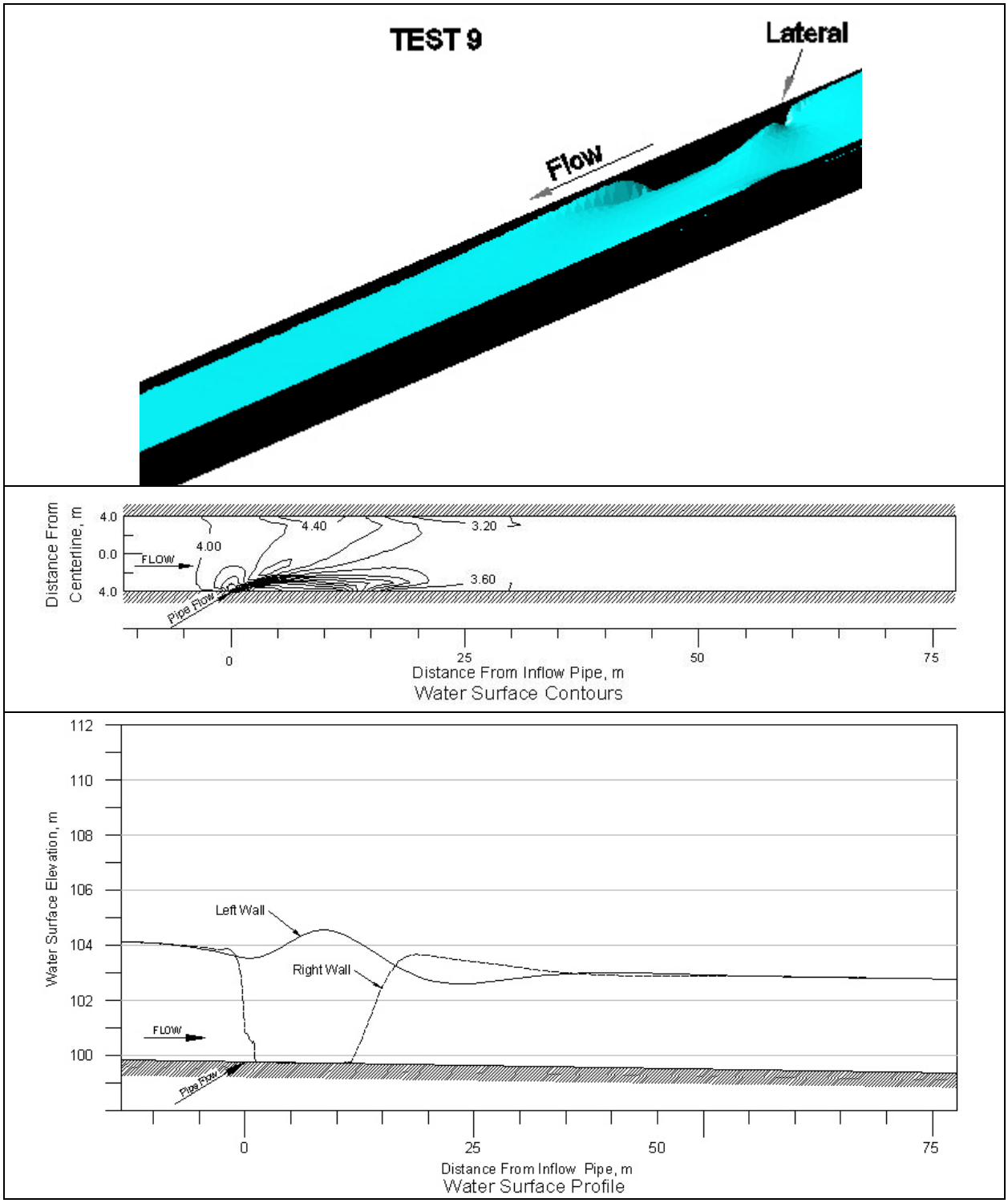

Figure 31. 2D MODEL results for Test 9.

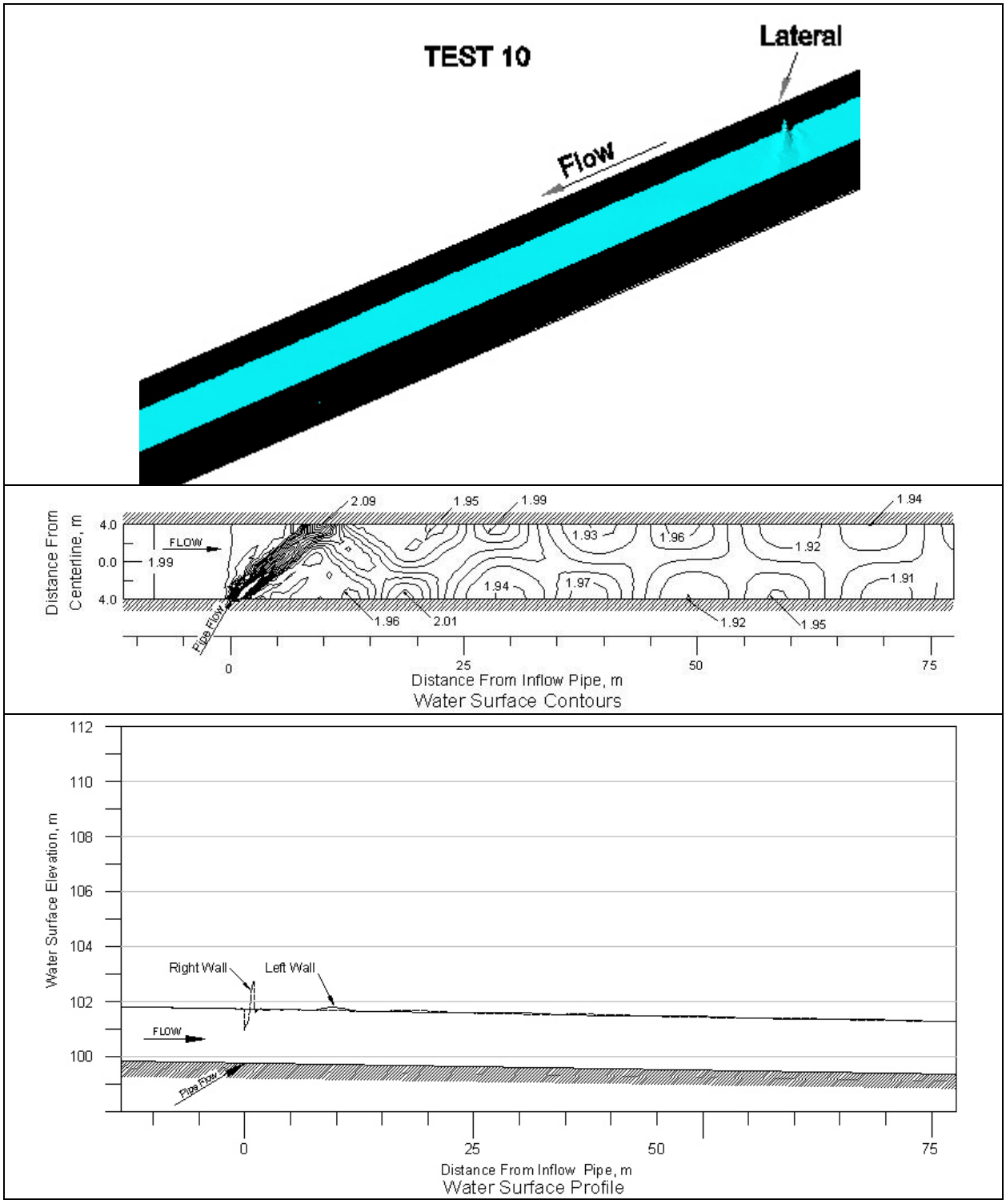

Figure 32. 2D MODEL results for Test 10.

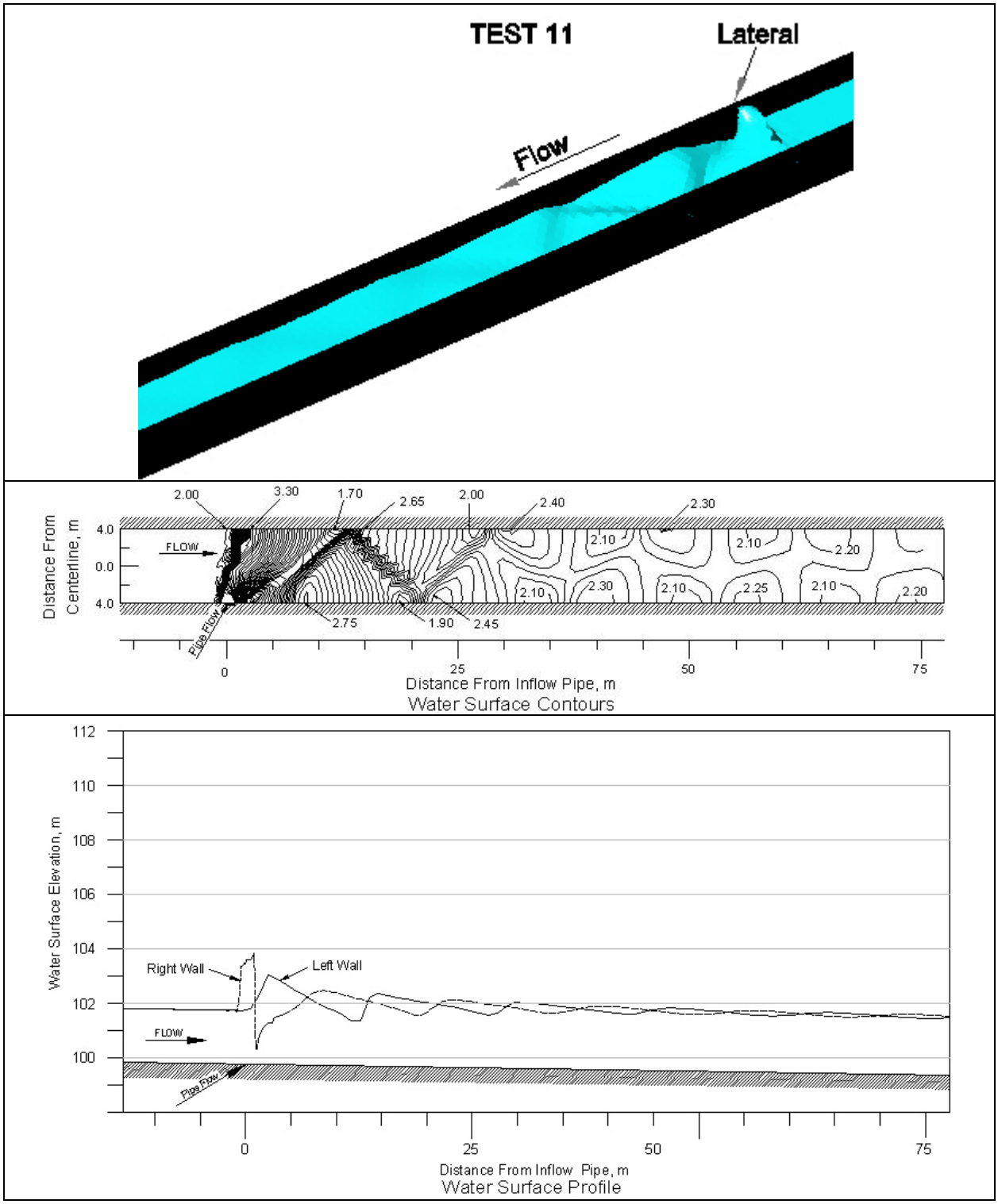

Figure 33. 2D MODEL results for Test 11.

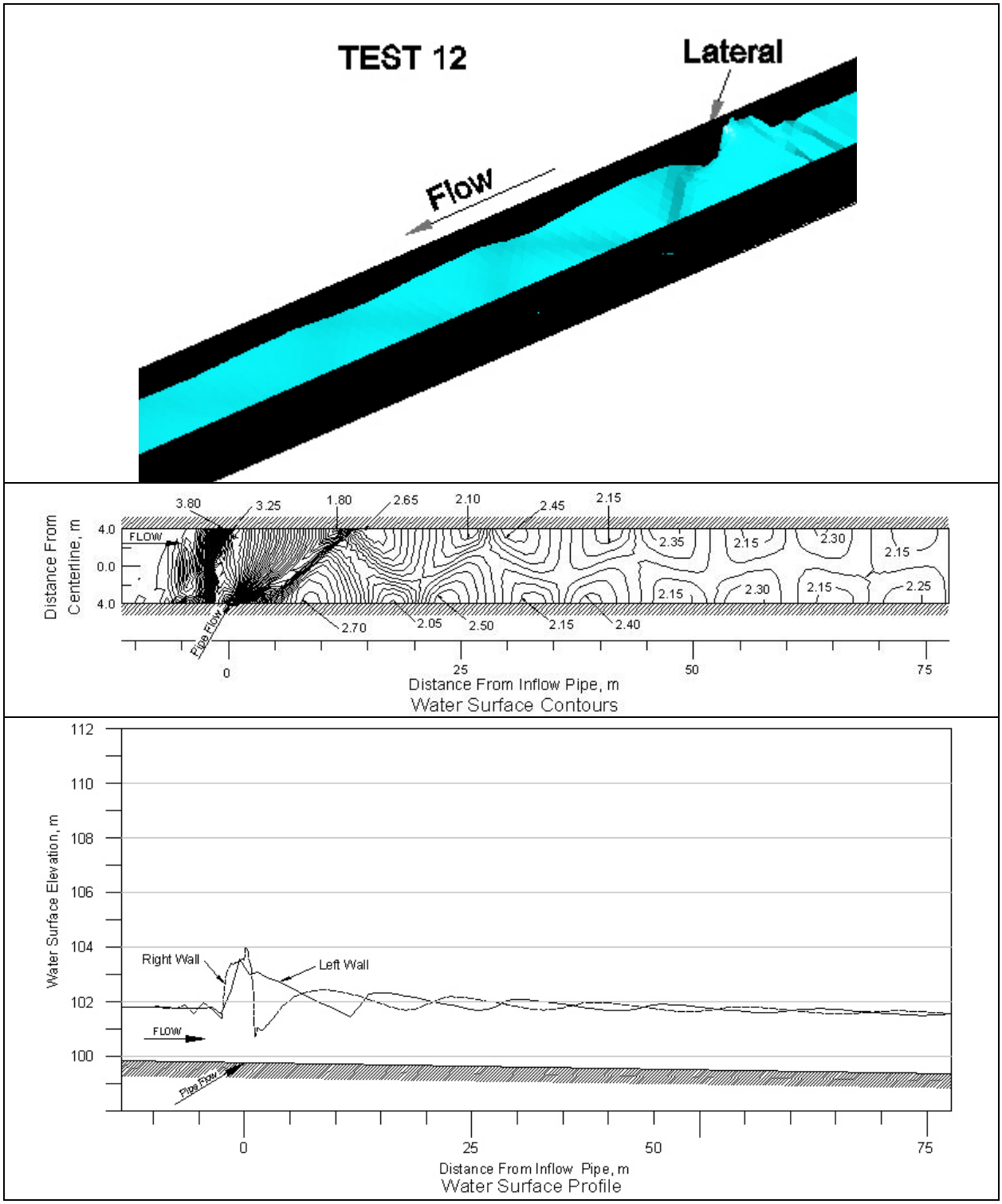

Figure 34. 2D MODEL results for Test 12.

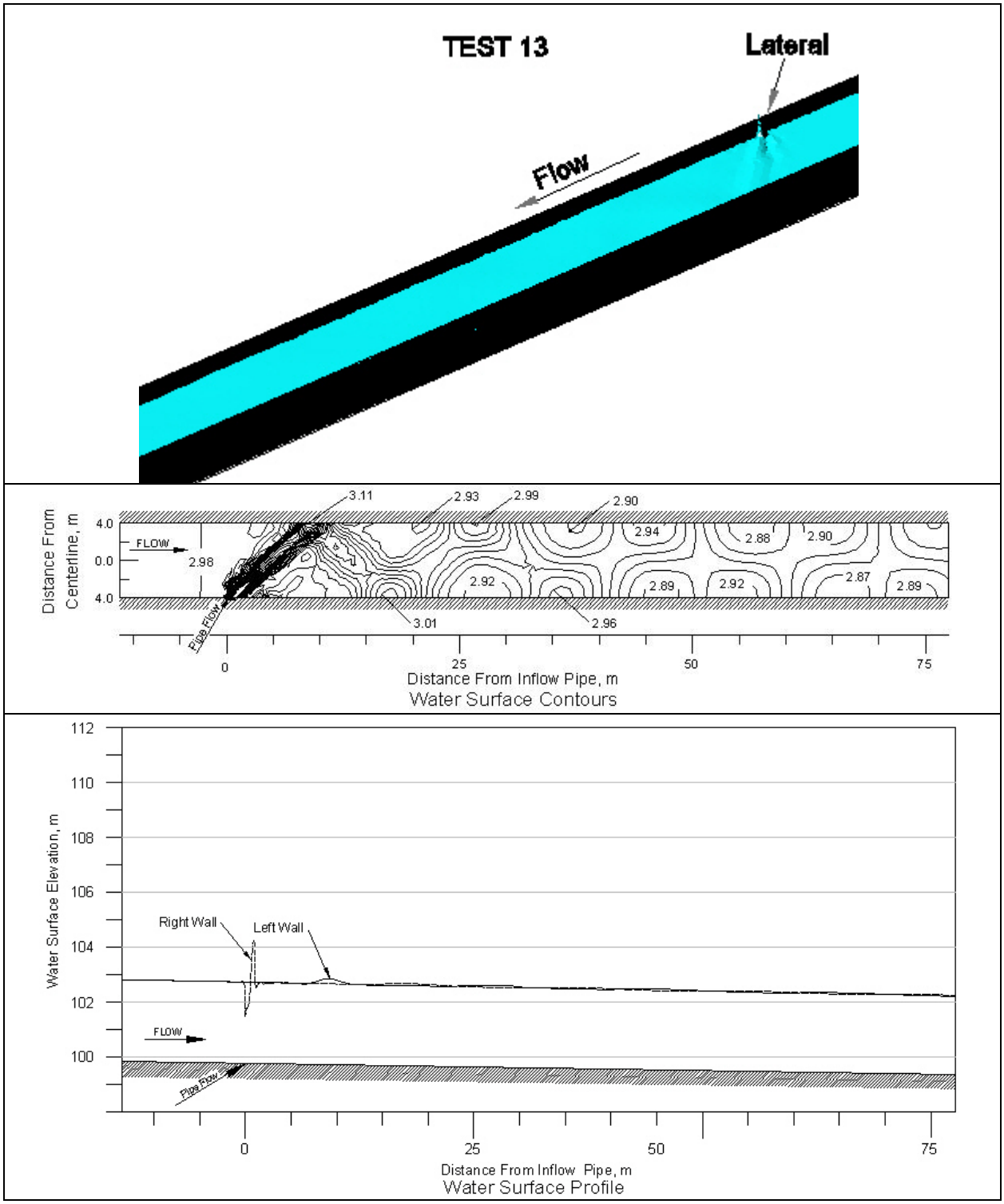

Figure 35. 2D MODEL results for Test 13.

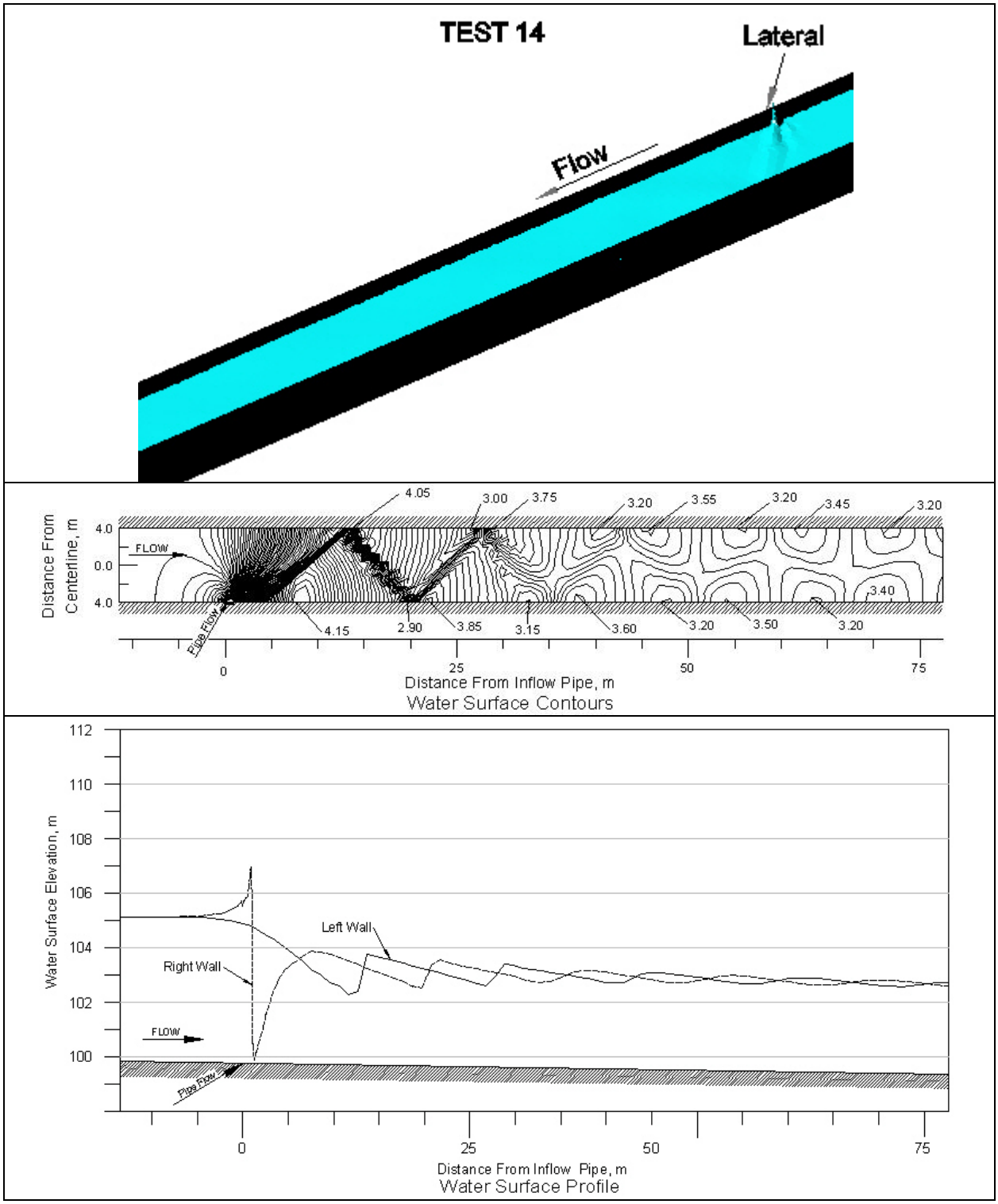

Figure 36. 2D MODEL results for Test 14.

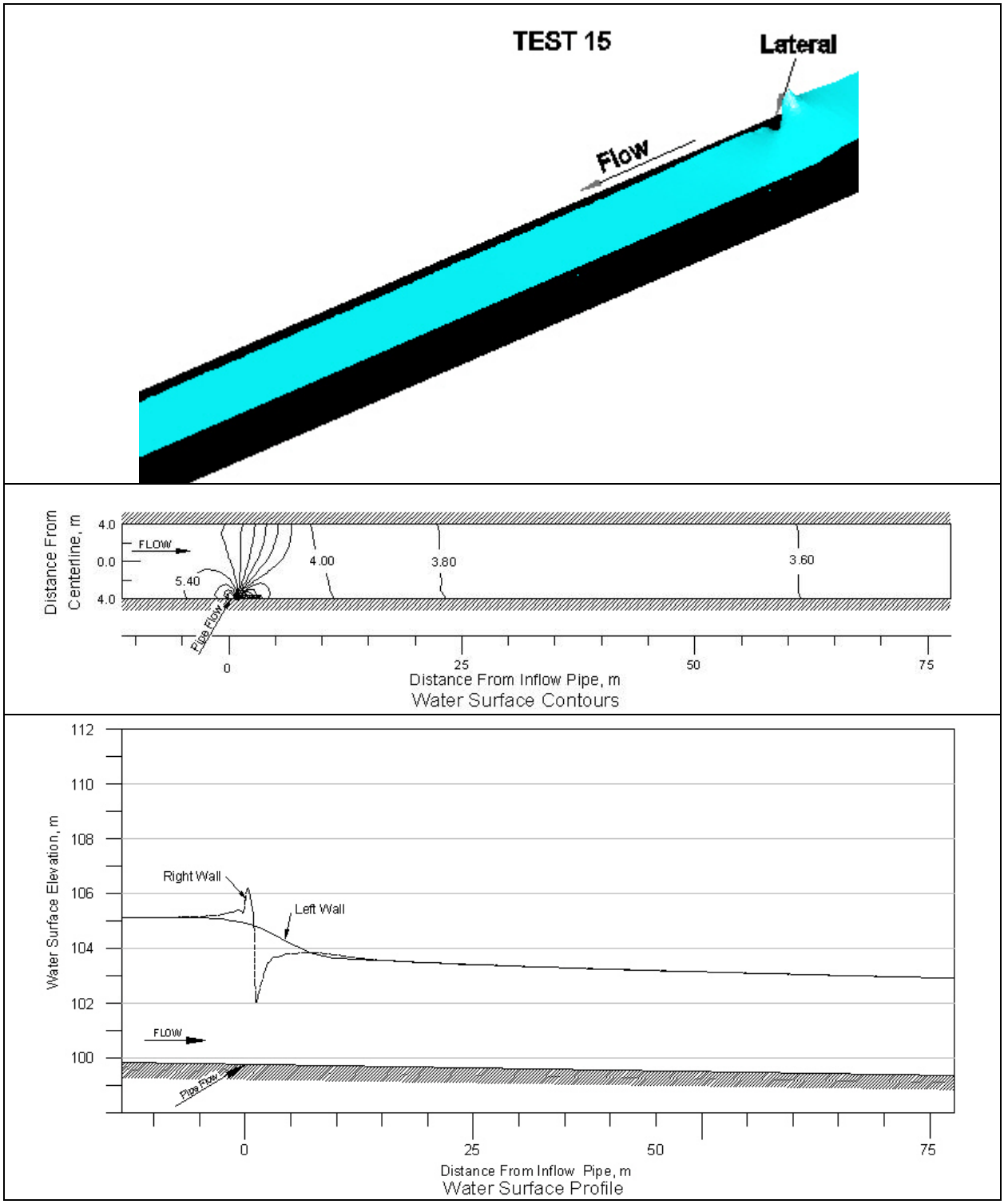

Figure 37. 2D MODEL results for Test 15.

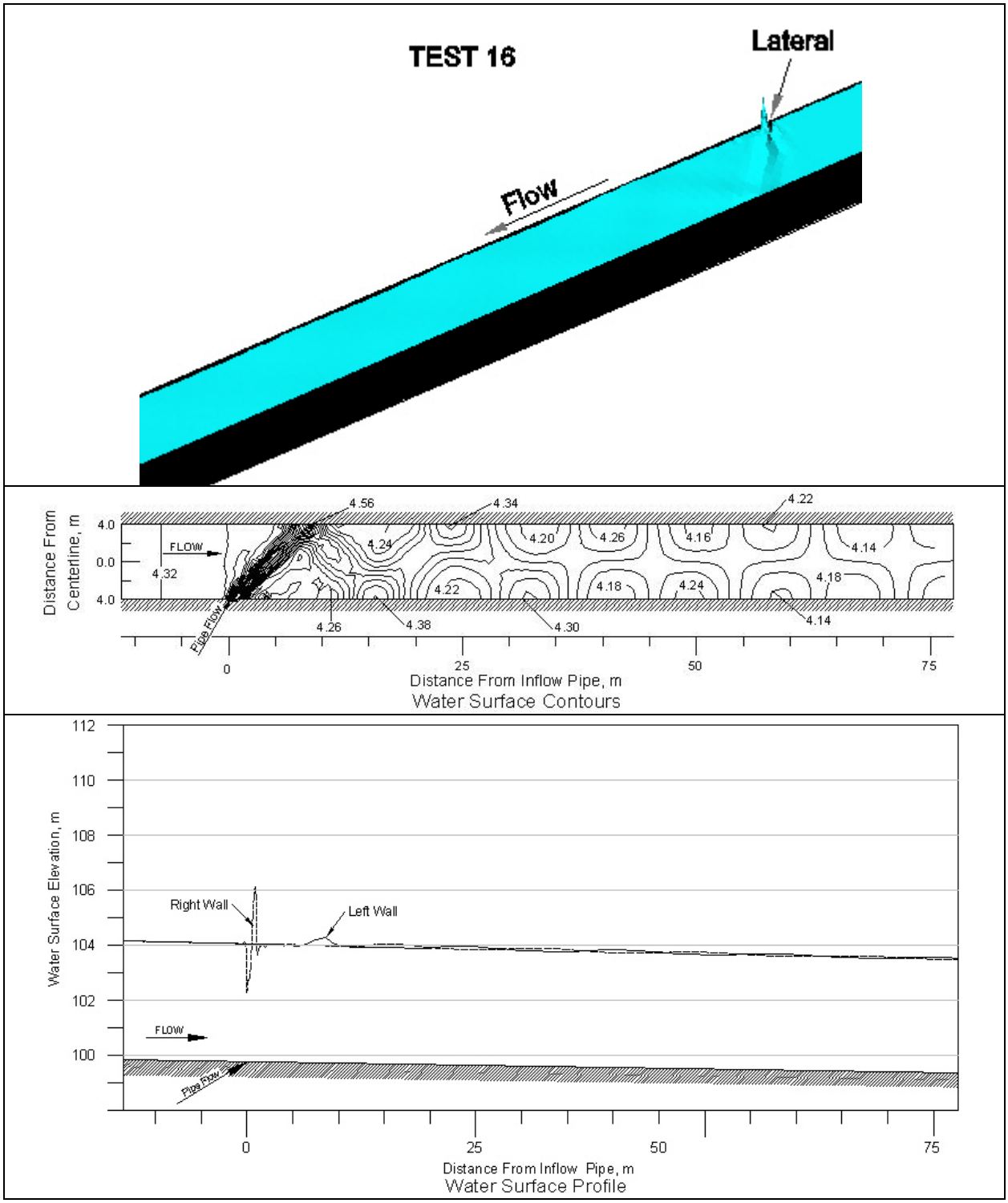

Figure 38. 2D MODEL results for Test 16.

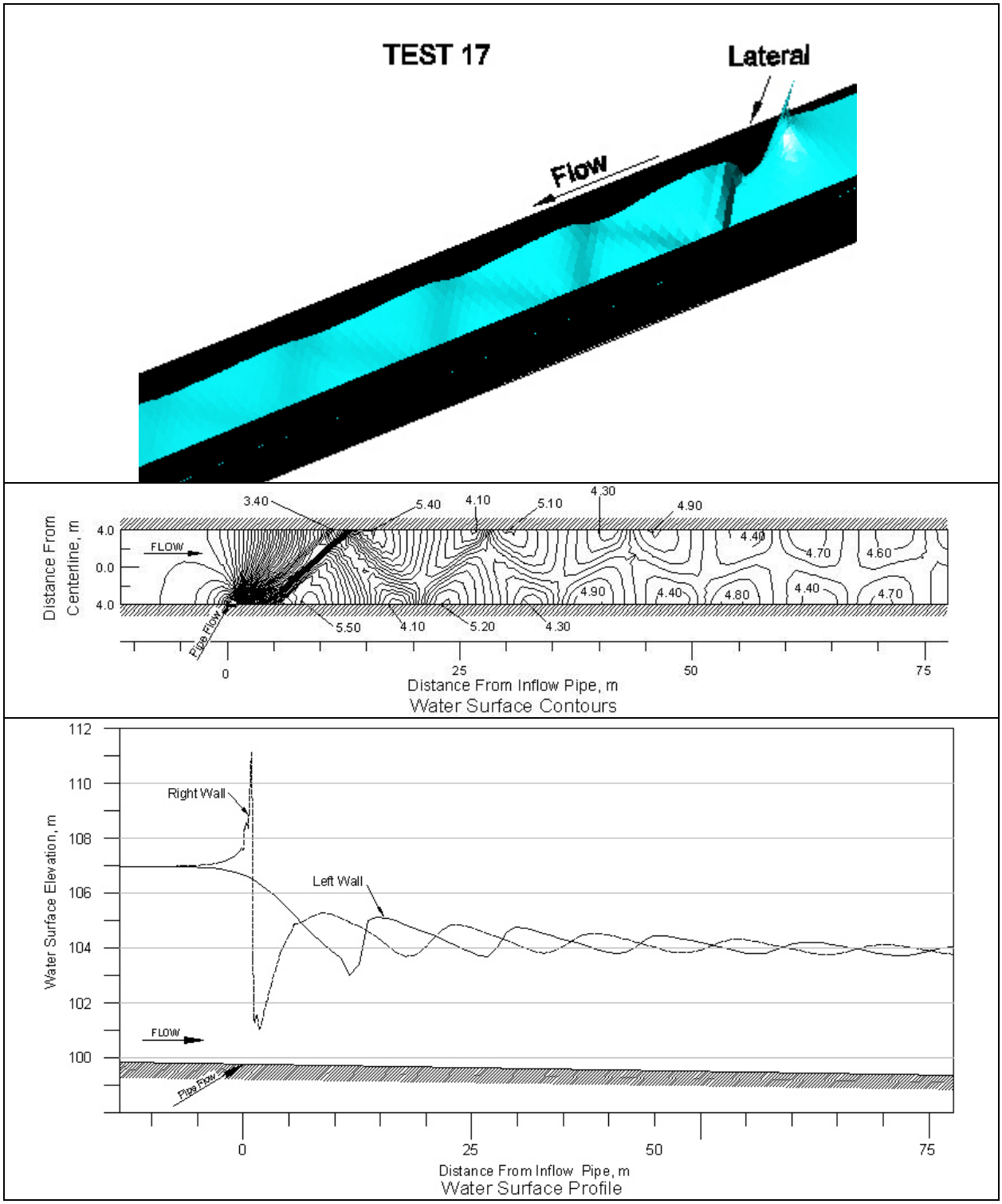

Figure 39. 2D MODEL results for Test 17.

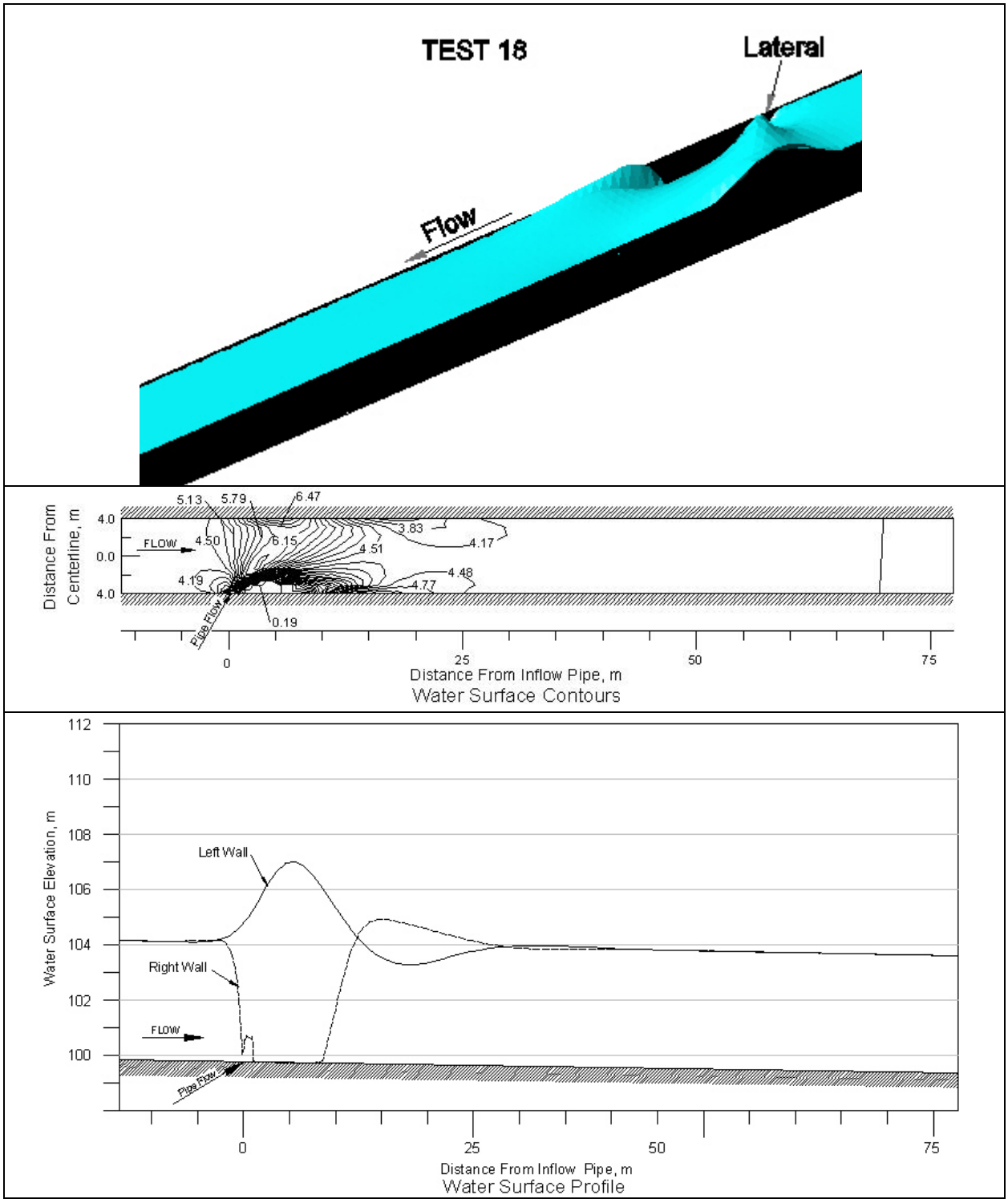

Figure 40. 2D MODEL results for Test 18.

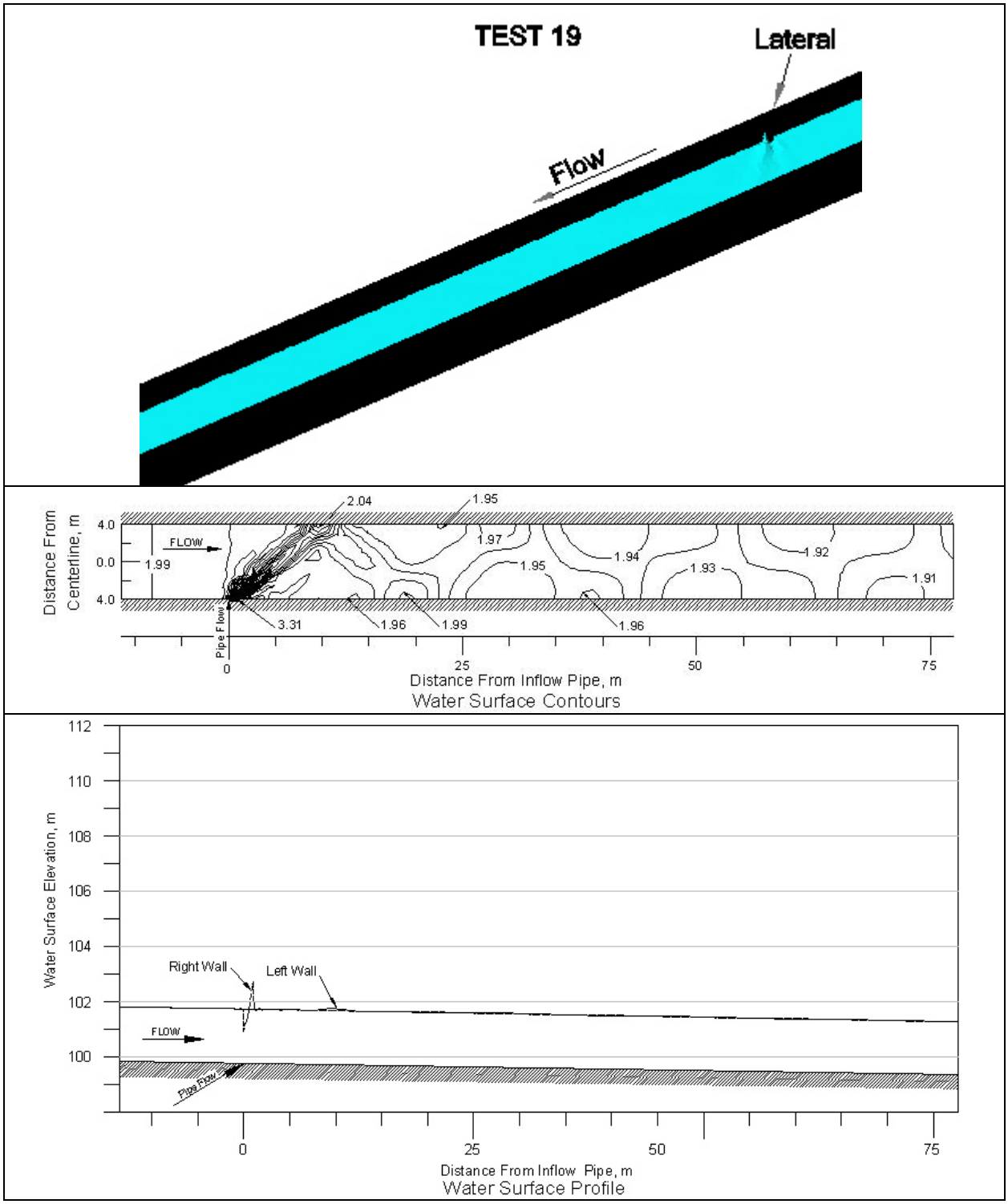

Figure 41. 2D MODEL results for Test 19.

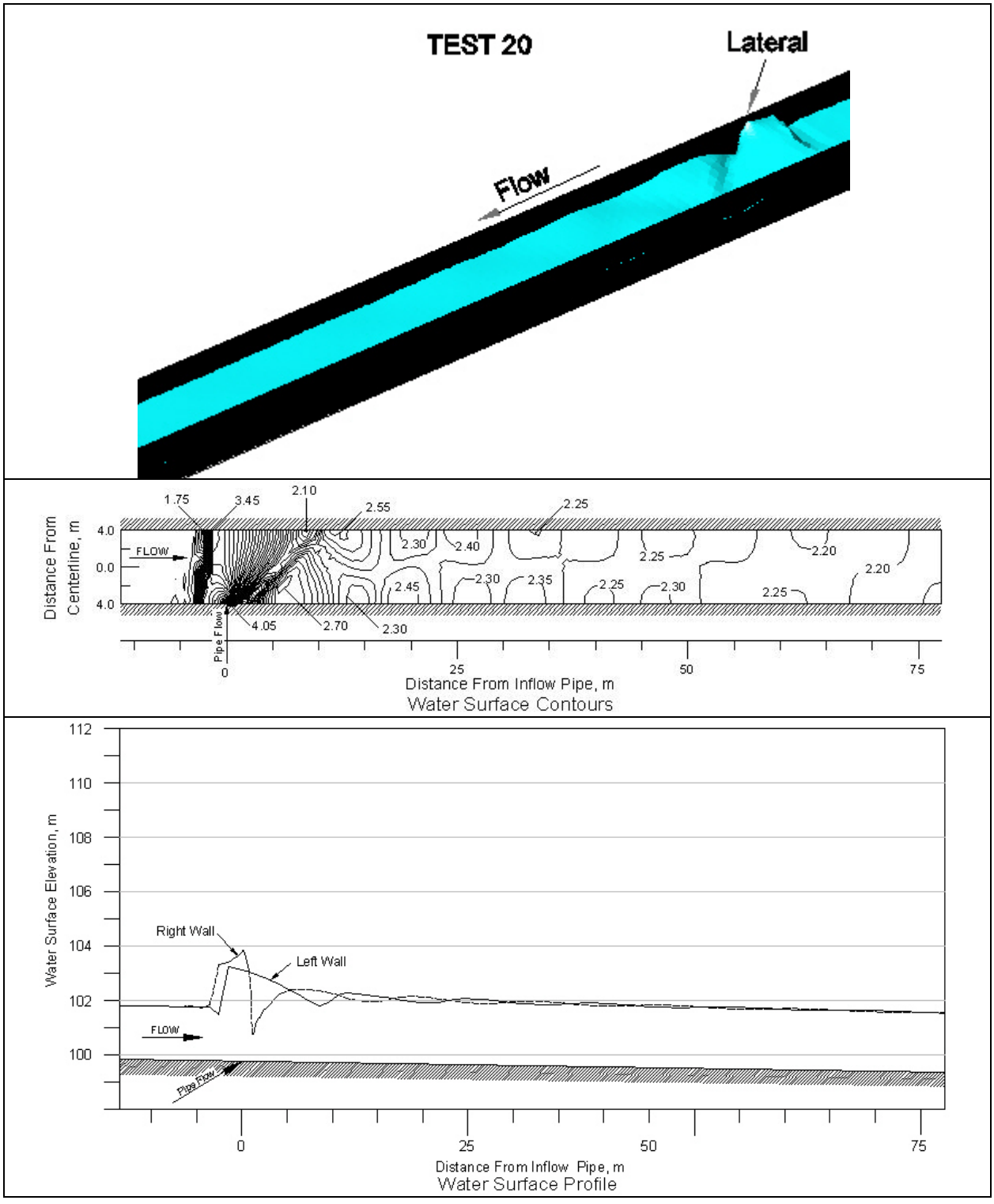

Figure 42. 2D MODEL results for Test 20.

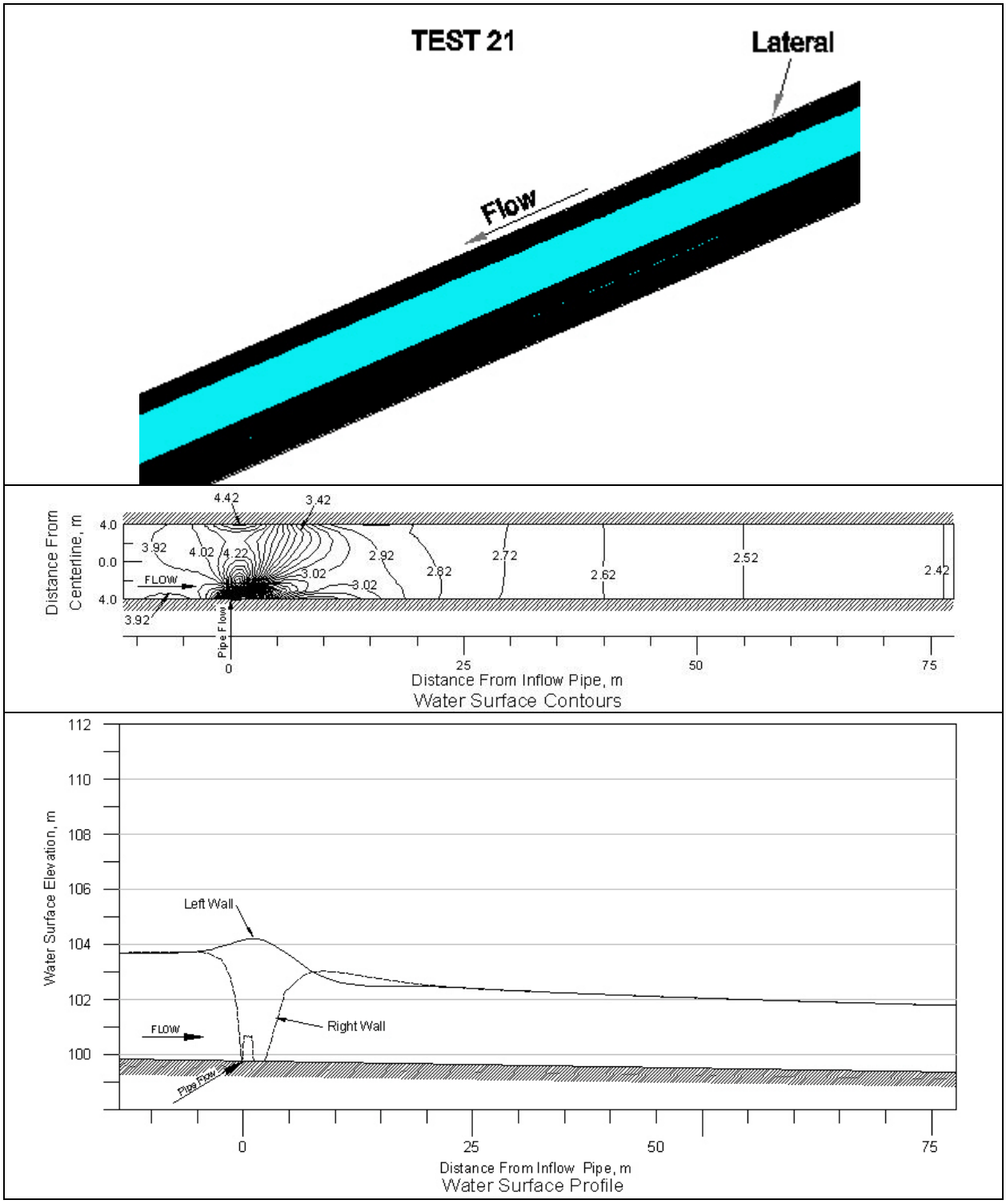

Figure 43. 2D MODEL results for Test 21.

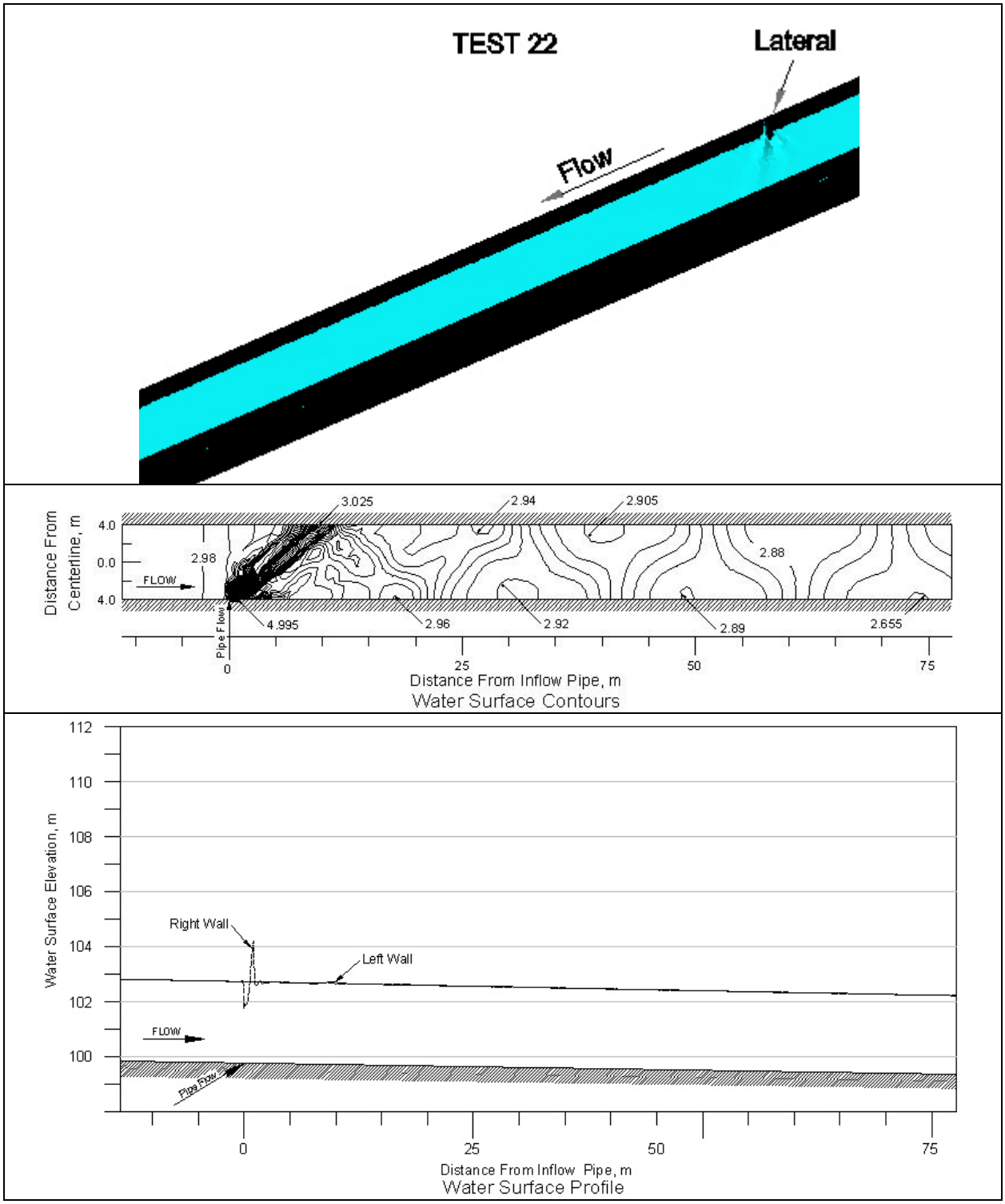

Figure 44. 2D MODEL results for Test 22.

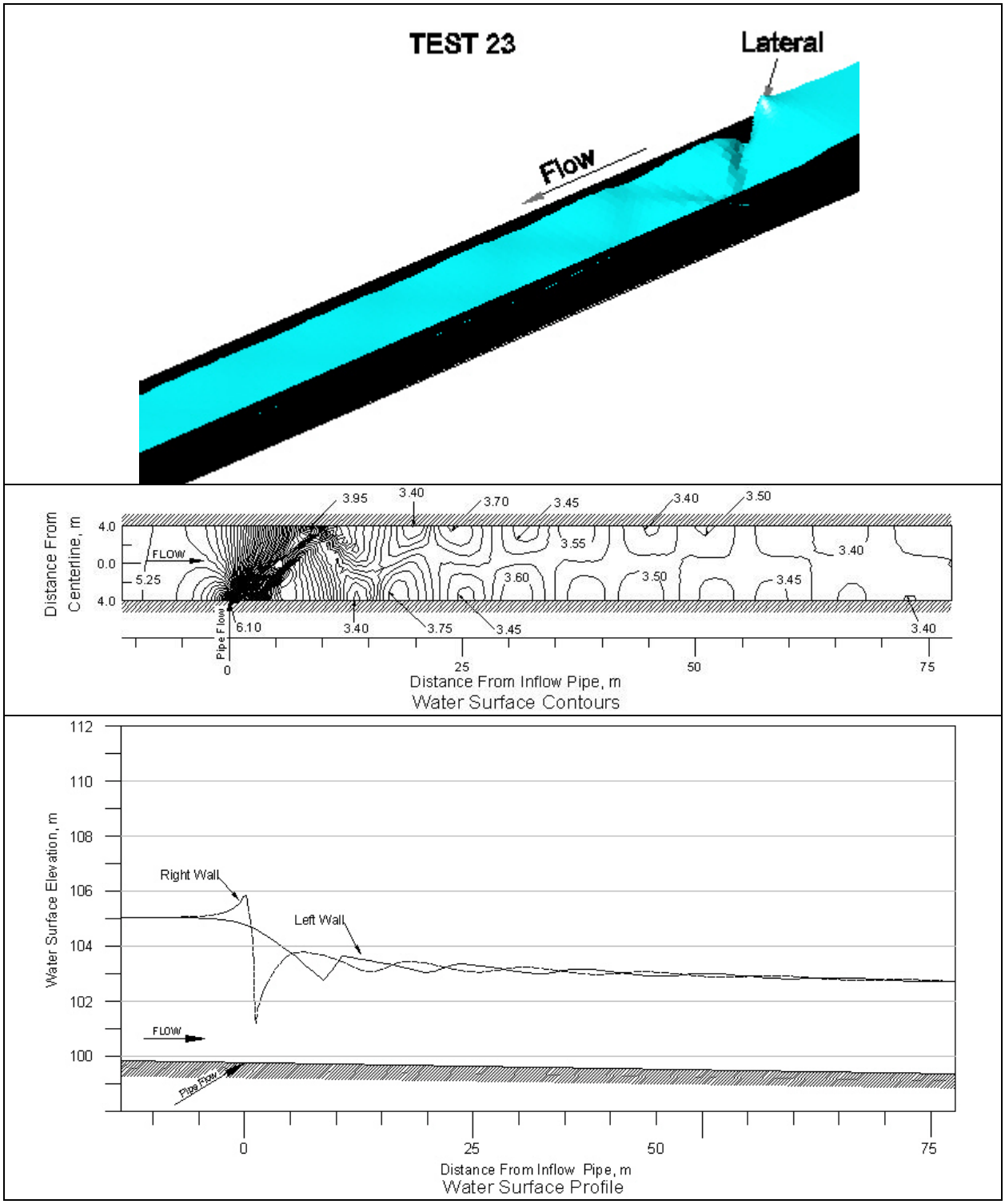

Figure 45. 2D MODEL results for Test 23.

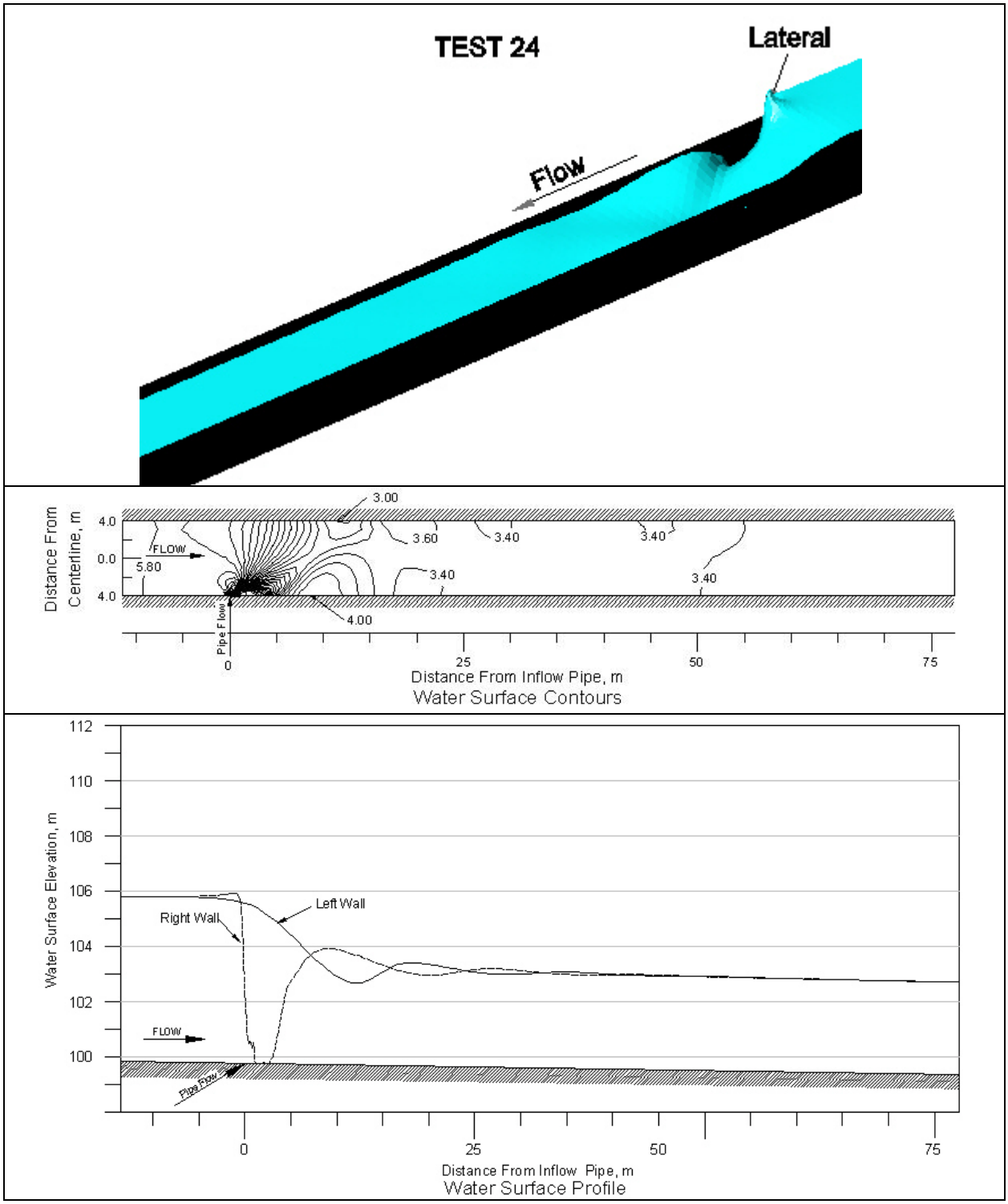

Figure 46. 2D MODEL results for Test 24.

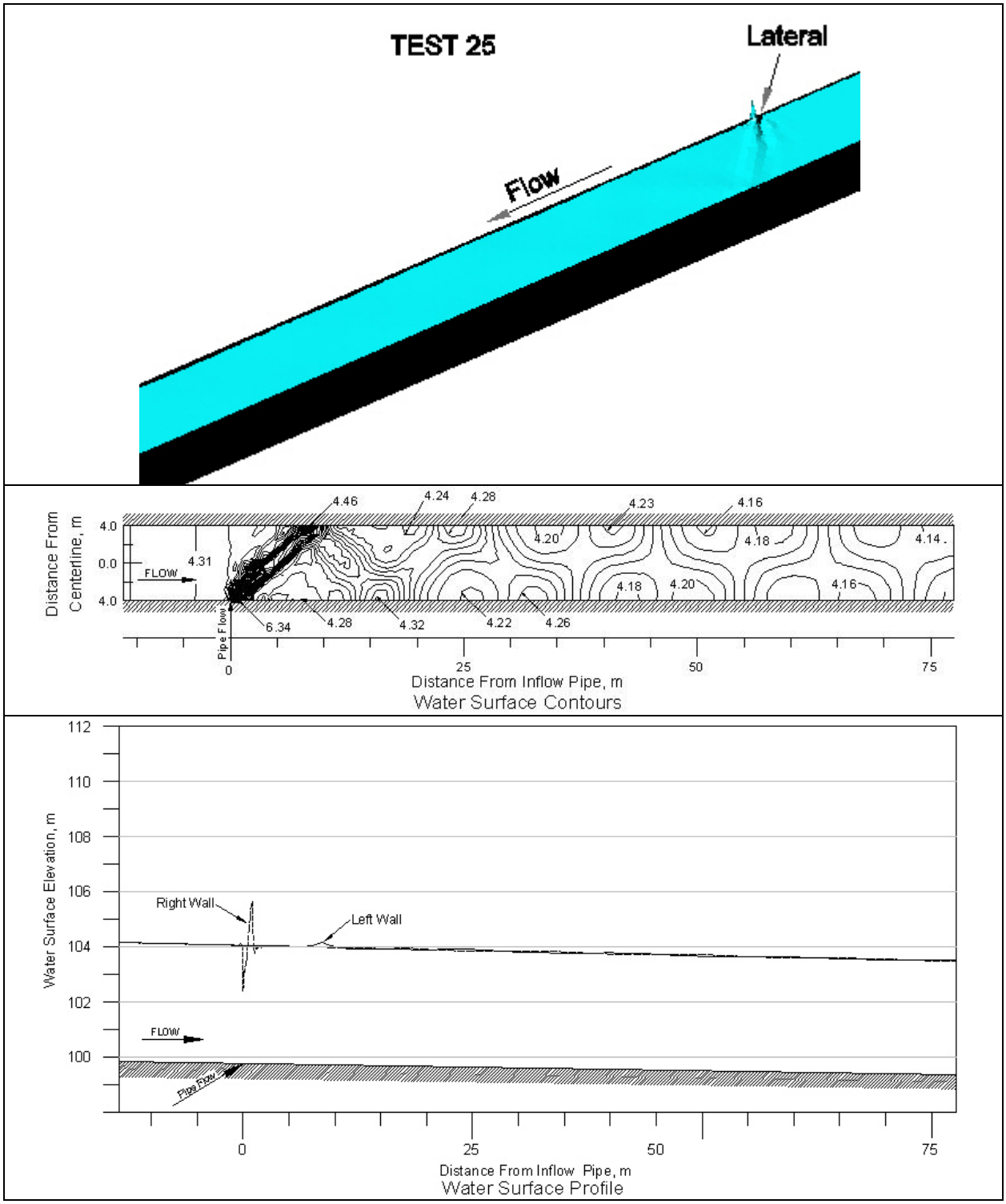

Figure 47. 2D MODEL results for Test 25.

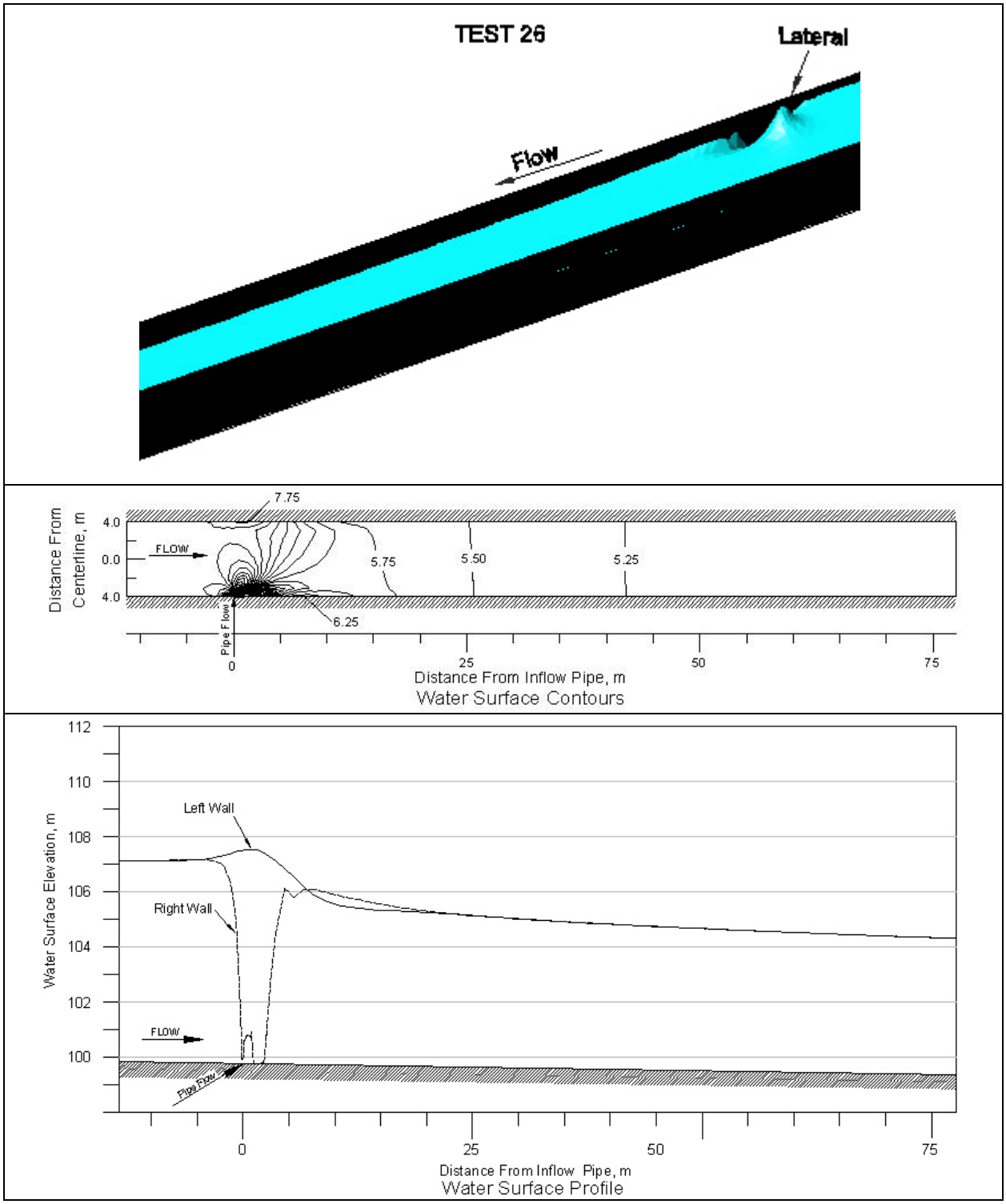

Figure 48. 2D MODEL results for Test 26.

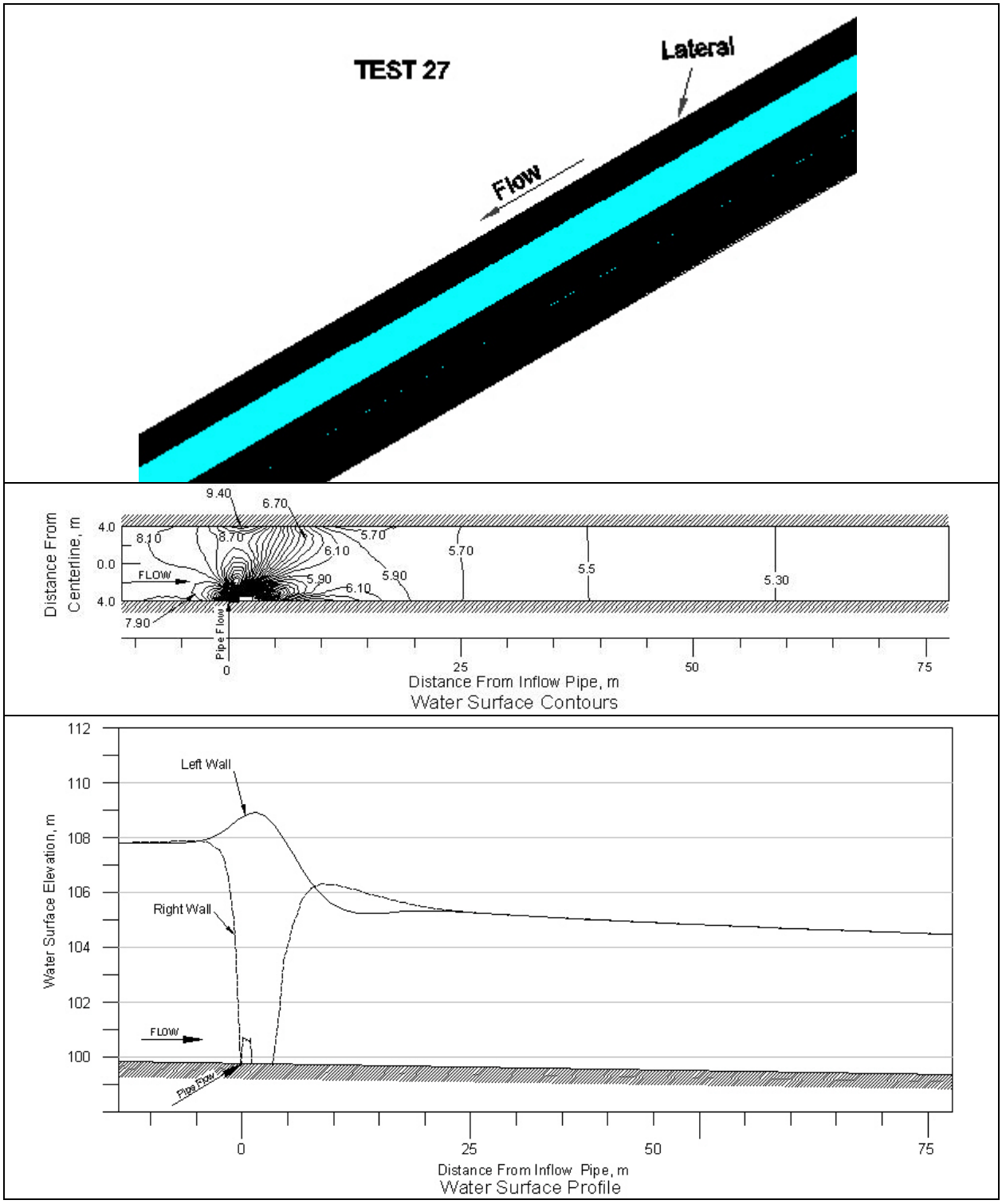

Figure 49. 2D MODEL results for Test 27.

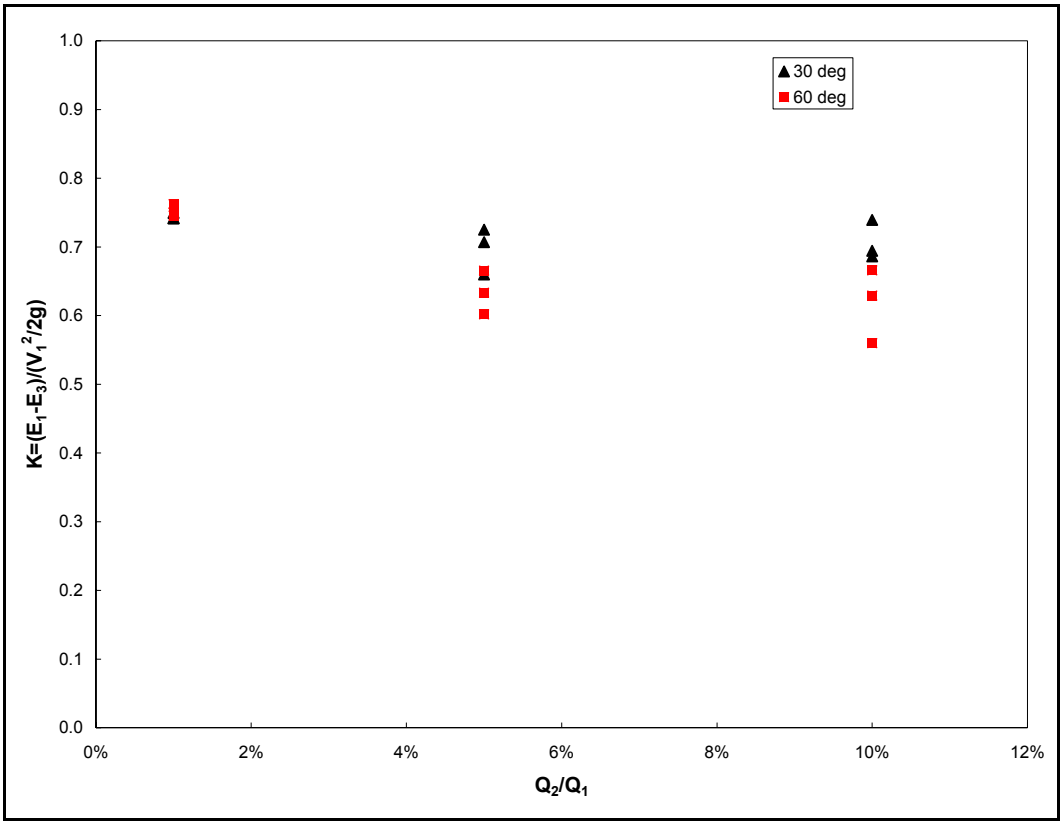

Figure 50. Energy loss coefficient for flow past a lateral.

Peak depth

The results of peak depths obtained from various laboratory studies are shown on Figure 51. The theoretical curve in Figure 51 is Equation 7. Those data plotted at L/b equal to zero are choked conditions where the Froude number is that for normal flow (i.e., not choked). Obviously, the data in Figure 51 show that the location of peak depths depends on more parameters than just Froude number. The peak depths are also plotted versus the discharge ratio, Q_2/Q_1, as shown on Figure 52. This plot provides little general information regarding peak depths.

As a side note, the 2D model is a finite element solution of the shallow-water equations, which assume hydrostatic pressure distribution. It is not surprising that the 2D results provide the same angle as that given in Equation 6 since they both are hydrostatic. However, Equation 6 ignores the effects of the lateral jet. So, for lateral angles (θ) less than that given by Equation 6, the 2D model gives the same L/b as Equation 6.

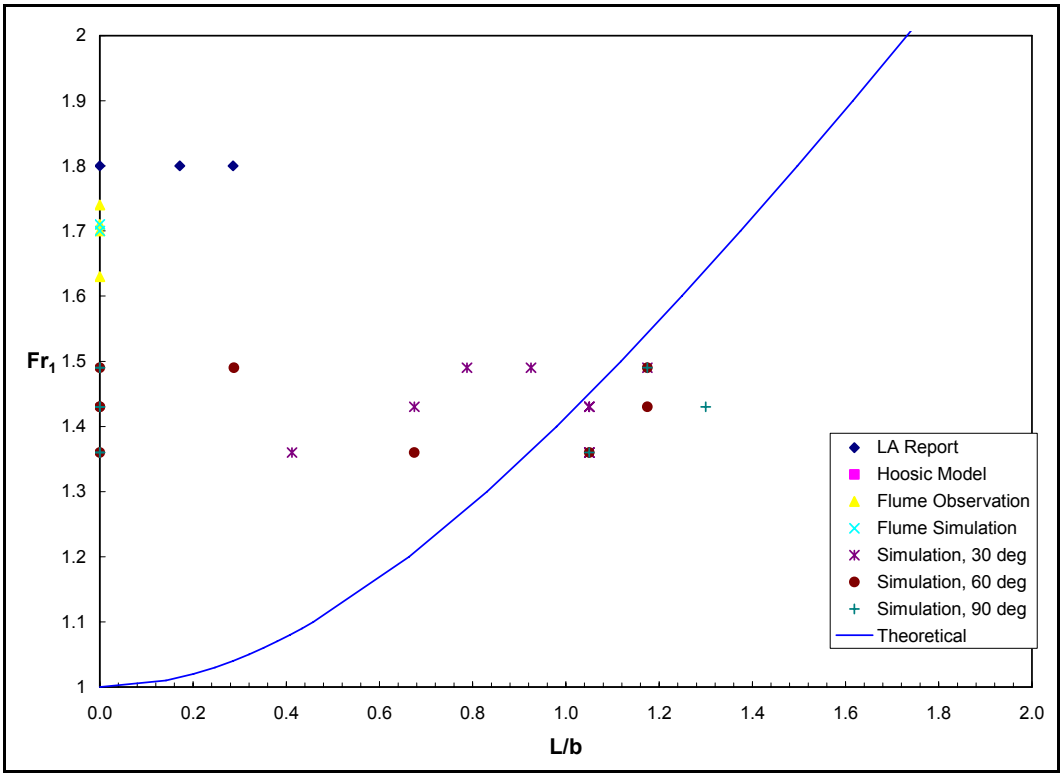

Figure 51. Location of peak depth as a function of upstream Froude Number.

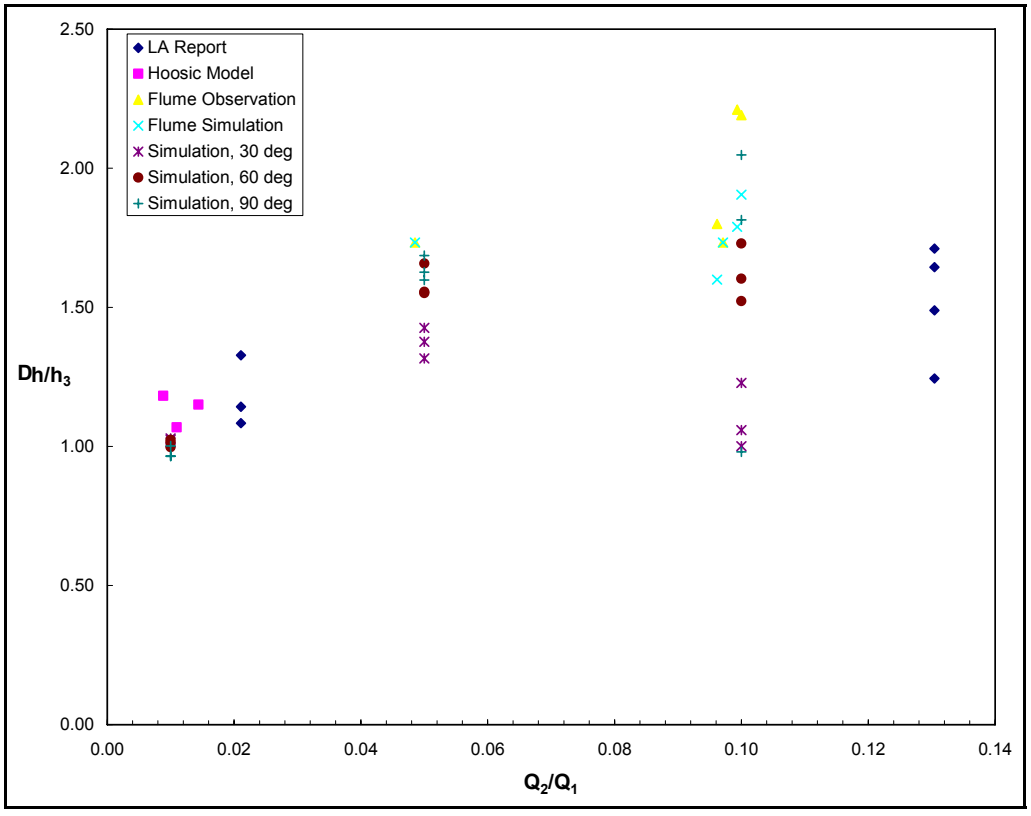

Figure 52. Peak depth as a function of flow ratio.

Peak depths that occur on the wall opposite the lateral flow's introduction were examined to determine the effects of culvert discharge, Froude number, and submergence. The limited data do not provide definitive results but might provide insight into which parameters are most important.

Location of peak depth

There are some data on maximum wave height at an open-channel supercritical flow junction. These data are gathered in Plate B-54 shown in Figure 10. However, data relating to lateral inflow are virtually nonexistent.

Momentum in the main channel has a substantial effect on the path of the issuing jet as it mixes with the channel flow. This is a three-dimensional problem, but a 2D model, under certain assumptions, can increase our understanding. The location of peak depth is presented from the various data sources in a dimensionless form, L/b, as shown in the data presented in Figure 51. Those data values at L/b equal to zero are associated with choked flow conditions where no oblique standing waves exist. The magnitudes of the peak depth are plotted relative to flow ratio, lateral angle, and submergence in Figures 52, 53, and 54, respectively. The plots show that there is no obvious correlation of peak depth to these parameters.

Another important consideration is the extent of oblique waves downstream from the lateral. The disturbance pattern will affect flow patterns at features such as bends and confluences downstream of the lateral. Also, the distance required to return to near-normal depth (i.e., wave damping) is key to designing wall heights required locally to contain standing waves. Comparison of laboratory data and 2D model results (Figures 18–21) shows that the numerical model damps waves too abruptly. This error is due to the hydrostatic pressure assumption in which vertical accelerations are neglected. The laboratory data suggest that a distance of at least 10 channel widths is required to re-establish relatively smooth flow downstream from the lateral.

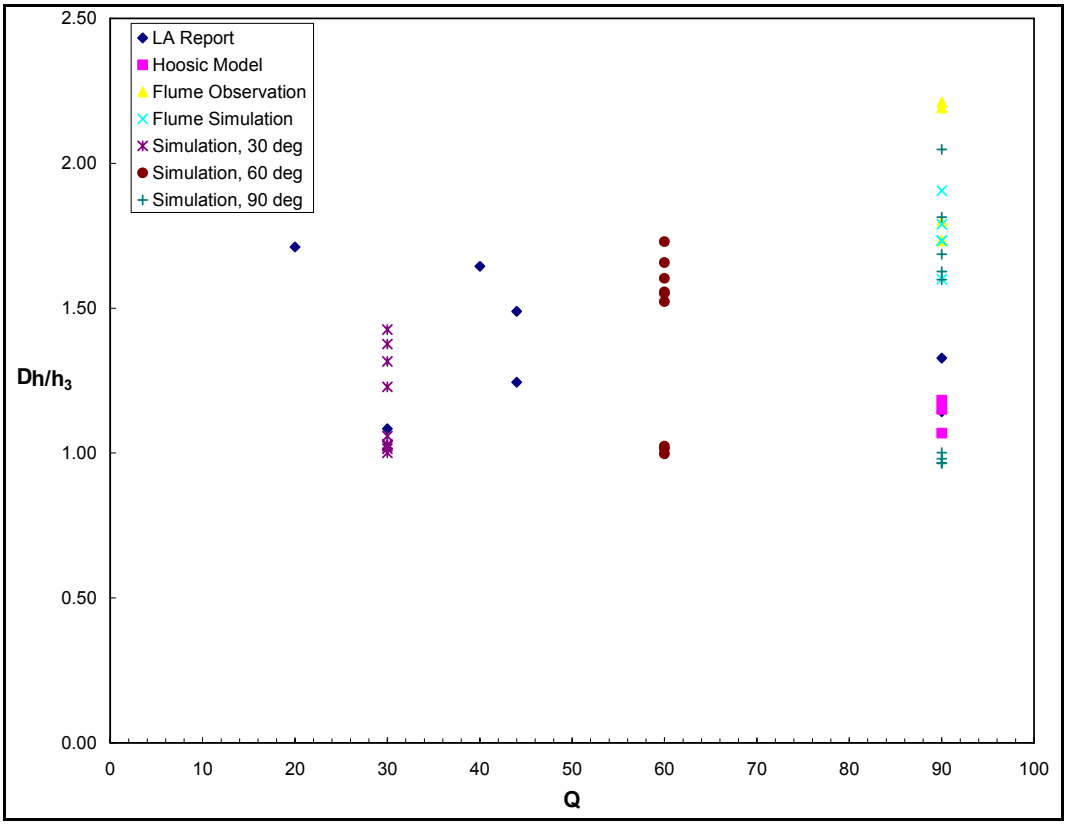

Figure 53. Peak depth as a function of lateral angle.

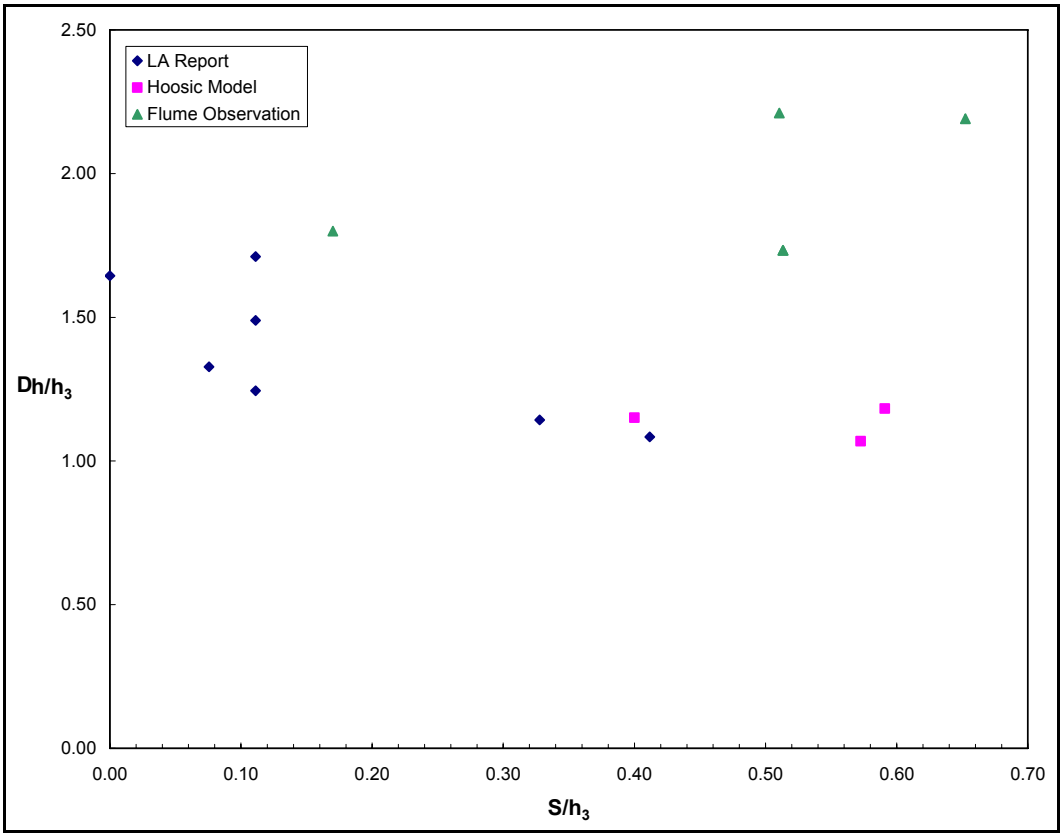

Figure 54. Peak depth as a function of submergence.

6 Summary

This study has investigated lateral flow introduced into rectangular man-made channels designed to convey supercritical flow. A series of laboratory experiments and numerical model results were presented. Various geometric and hydraulic conditions were studied to evaluate hydraulic variables such as location and magnitude of peak depths. This depth information is necessary for determining channel wall heights required to contain flows in the vicinity of laterals.

Findings

A 2D model does a reasonable job of simulating the flow depths associated with main channel/lateral flow interaction. The model reproduces the oblique standing wave generated by the lateral flow. However, the length of the wave is too short (angles too large) due to the hydrostatic assumption. This fact is well established in the literature (e.g., Berger and Stockstill 1995; Bhallamudi and Chaudhry 1992; Kruger and Rutschmann 2006). A 2D model also provides lateral variation of flow depths and computes the peak depth with reasonable accuracy. The 2D model, although it ignores vertical inertia and is only a depth-averaged representation, does capture the choked condition and the return to supercritical flow downstream of the junction. A key attribute of the numerical model is its ability to identify unsatisfactory flow conditions and the need for hydraulic design refinements.

This study provides hydraulic design information for lateral inflow into rectangular channels conveying supercritical flow. The head loss experienced by the main-channel flow as it crosses lateral inflow (Equation 3) can be estimated using a loss coefficient 0.7. This coefficient is an average value for all lateral angles and discharge ratios examined. Oblique standing waves are generated at a lateral when the flow is supercritical. The local depth in this wave pattern can be significantly larger than the normal depth. Data from laboratory experiments suggest that a distance of at least 10 channel widths is required to re-establish relatively smooth flow downstream from a lateral.

Recommendations for further study

A systematic flume study must be conducted to evaluate and quantify the effects of each of the governing parameters listed in this report. Such a laboratory study was beyond the scope of the current project. However, since the parameters and flow mechanics have been established, a laboratory study should prove to be quite valuable. The effects of submergence, flow ratio, channel width, and lateral angle can be quantified with experiments.

The current study was directed solely toward conditions in rectangular channels. Since many high-velocity channels are trapezoidal, perhaps lateral inflow onto side slopes should be investigated. This would require a flume study and additional testing of a numerical model's abilities. Trapezoidal channels are more difficult to simulate because of run up on the side slopes. The domain limit is not known *a priori* because the flow width depends on the flow depth. A parallel study similar to the one addressing rectangular channels could be conducted for trapezoidal channels conveying supercritical flow.

References

Berger, R. C., and R. L. Stockstill. 1995. Finite-element model for high-velocity channels. *Journal of Hydraulic Engineering* 121 (10): 710-716.

Bhallamudi, S. M., and M. H. Chaudhry. 1992. Computation of flows in open-channel transitions. *Journal of Hydraulic Research* 30 (1): 77-93.

Ippen, A. T. 1951. Mechanics of supercritical flow. *Transactions of the American Society of Civil Engineers* 116: 268-295.

Kruger, S., and P. Rutschmann. 2006. Modeling 3D supercritical flow with extended shallow-water approach. *Journal of Hydraulic Engineering* 132 (9): 916-926.

Ohtsu, I., Y. Yasuda, and H. Gotoh. 2003. Flow conditions of undular hydraulic jumps in horizontal rectangular channels. *Journal of Hydraulic Engineering* 129 (12): 948-955.

U.S. Army, Office, Chief of Engineers. 1991. *Hydraulic design of flood control channels*. Engineer Manual No. 1110-2-1601. Washington, DC.

U.S. Army Engineer District, Los Angeles. 1960. *Typical side drains; hydraulic model investigation*. Report No. 2-101. Los Angeles, CA.

U.S. Army Engineer District, Los Angeles. 1964. *Walnut Creek Channel and side drains; hydraulic model investigation*. Report No. 2-104. Los Angeles, CA.

U.S. Army Engineer Waterways Experiment Station. 1962. *Flood-control project Hoosic River, North Adams, Massachusetts, hydraulic model investigation*. Technical Memorandum No. 2-338. Vicksburg, MS.

Appendix A: Notation

The following symbols are used in this report:

A = flow area
b = channel width
d = diameter of lateral
g = gravitational acceleration
h = cross-sectional average depth in the channel
K = energy loss coefficient
n = Manning's roughness coefficient
P = distance between lateral invert and channel invert
Q = discharge
S = submergence of lateral
S_o = bed slope
V = cross-sectional average velocity in the channel
z = invert elevation of the channel
α = energy correction factor
β = wave angle
δ = momentum correction factor
ΔE = energy loss
θ = angle of the lateral
ρ = density of water

Subscripts 1, 2, and 3 refer to the channel upstream of the lateral, the lateral, and the channel downstream of the lateral, respectively.

REPORT DOCUMENTATION PAGE

Form Approved
OMB No. 0704-0188

1. REPORT DATE *(DD-MM-YYYY)*	2. REPORT TYPE	3. DATES COVERED *(From - To)*
September 2007	Final report	

4. TITLE AND SUBTITLE

Lateral Inflow in Supercritical Flow

5a. CONTRACT NUMBER

5b. GRANT NUMBER

5c. PROGRAM ELEMENT NUMBER

6. AUTHOR(S)

Richard L. Stockstill

5d. PROJECT NUMBER

5e. TASK NUMBER

5f. WORK UNIT NUMBER

7. PERFORMING ORGANIZATION NAME(S) AND ADDRESS(ES)

U.S. Army Engineer Research and Development Center
Coastal and Hydraulics Laboratory
3909 Halls Ferry Road, Vicksburg, MS 39180-6199

8. PERFORMING ORGANIZATION REPORT NUMBER

ERDC/CHL TR-07-10

9. SPONSORING / MONITORING AGENCY NAME(S) AND ADDRESS(ES)

U.S. Army Corps of Engineers
Washington, DC 20314-1000

10. SPONSOR/MONITOR'S ACRONYM(S)

11. SPONSOR/MONITOR'S REPORT NUMBER(S)

12. DISTRIBUTION / AVAILABILITY STATEMENT

Approved for public release; distribution is unlimited.

13. SUPPLEMENTARY NOTES

14. ABSTRACT

Lateral culverts are used to introduce storm drain flow into urban channels if the culvert flow is less than 10 percent of the main channel flow. Confluences of supercritical flow are complicated by standing waves that are generated at boundary alignment changes. The confluence addressed in this report is the case where culvert flow is introduced into a rectangular-shaped channel via a lateral. Even when the culvert discharge is less than 10 percent of the main channel flow, the momentum effects can produce significant bulking of the main channel flow. An understanding of the flow conditions in the vicinity of laterals is essential in an economical design of these structures. The current research evaluated a modeling method to determine if it is appropriate for simu¬lating the flow depth increases attributed to lateral inflows in high-velocity channels. This report describes a series of laboratory experiments followed by numerical simulations. Following model validation, various geometric and hydraulic conditions were studied to evaluate hydraulic conditions such as location and magnitude of peak depths. Knowledge of these flow conditions is necessary for hydraulic design of channel walls (height and length) required to contain flows in the vicinity of laterals.

15. SUBJECT TERMS

Clark County, Nevada
Flood-control channels
Hydraulic design
Lateral inflow
Supercritical flow

16. SECURITY CLASSIFICATION OF:			17. LIMITATION OF ABSTRACT	18. NUMBER OF PAGES	19a. NAME OF RESPONSIBLE PERSON
a. REPORT	b. ABSTRACT	c. THIS PAGE			19b. TELEPHONE NUMBER *(include area code)*
UNCLASSIFIED	UNCLASSIFIED	UNCLASSIFIED		77	